# SCALING ANALYSIS OF ACID ROCK DRAINAGE

## MEND Project 1.19.2

**This work was done on behalf of MEND and sponsored by Environment Canada**

**October 1995**

# SCALING ANALYSIS OF ACID ROCK DRAINAGE

by

**M. Otwinowski**
*Synergetic Technology*
**139, 31-Avenue N.W.**
**Calgary, Alberta T2M 2P1**
**Telephone: (403) 220 9576**

**REPORT PREPARED FOR**

**MINE ENVIRONMENT NEUTRAL DRAINAGE PROGRAM**

**and**

**ENVIRONMENT CANADA**

TABLE OF CONTENTS

## ACKNOWLEDGEMENTS

The guidance by Benoit Godin, Section Head, Environmental Contaminants Division, Pacific and Yukon Region, Environment Canada, who provided several ideas and continued support for this project is gratefully acknowledged. This project benefited greatly from discussions and information provided by M. Blanchette, P. Gelinas, K. Ferguson, P. Grabinski, B. Krusche, R. Lefebvre, G.W. Luther III, R. McCandless, M.A. McKibben, K.A. Morin, R.V. Nicholson, W.A. Price, A. Robertson, I. Suzuki, G.A. Tremblay, J. Weres and W.W. White III. The reviewers of the draft report; Stephen Day, Benoit Godin, and Ronald V. Nicholson supplied helpful comments and suggestions.

## EXECUTIVE SUMMARY

The highly nonlinear nature of the kinetic equations describing the coupled geochemical and physical processes involved in pyrite oxidation has posed serious questions about the predictability of the environmental impact of acid rock drainage. In response to these questions this report describes the results of a research project which has been initiated with the purpose to provide a quantitative analysis of the interrelated elementary chemical and physical processes which are responsible for pyrite oxidation and acid rock drainage (ARD). This project is part of an effort to design practical indicators which would combine quantitative laboratory data, obtained for small samples of waste rock, with large-scale effects observed in waste rock piles.

The main objective of this project was to determine the simple scaling laws which govern the geochemical and thermodynamic behaviour of pyritic rock in waste rock piles. The scaling indicator $\delta$ which combines information about processes occurring at different scales, is an innovative feature of this project.

Effective kinetic equations for coupled chemical reactions involved in pyrite oxidation have been derived. The concentration of dissolved oxygen has been described by a simple formula which gives reasonable quantitative agreement with experimental data for the whole range of temperatures and oxygen concentrations in the gas phase, as required for ARD analysis. The strong decrease of dissolved oxygen concentration with temperature is included in the model. This property has not been included in previous models - the omittance of which could result in an overestimation of the acid generation potential.

Energy and oxygen transport are described by using a reaction-transport model. Strong nonlinear dependence of the effective reaction rates on the physical, mineralogical and chemical parameters has been described by means of a scaling parameter $\delta$ which can be used as a practical indicator of ARD for waste rock piles. The dimensionless scaling parameter $\delta$ combines information about pile porosity, pile size, effective reactive surface area, temperature dependence of the rate of pyrite oxidation, oxygen diffusion in the gas phase, heat of the pyrite oxidation reaction, thermal conductivity of waste rock, and ambient temperature.

The sensitivity analysis provides information about the required accuracy of experimental tests and the relative importance of parameters governing different physical and geochemical processes responsible for ARD. In particular, it is shown that the effectiveness of impermeable covers increases with the pyrite concentration.

The scaling analysis indicates that geochemical and transport processes operate at the meso-scale in a way fundamentally different from the full-scale. Critical values of the scaling parameter $\delta$, at which bifurcation's or *thermodynamic catastrophes* leading to accelerated acid generation rates, have been determined for different scenarios. The critical dependence of ARD on pile porosity, pile size and reactive surface area is one of the conclusions of the bifurcation analysis. The results of the scaling analysis offer the possibility of a cheap and fast preliminary assessment of the expected environmental impact.

All parameters and variables of the present model can be measured in independent experiments. The model produces realistic results for acid generation rates without introducing adjustable fitting parameters used by all (known to us) other waste rock models. Several results of this study are significantly different from conclusions and assumptions of other existing models.

Quantitative results presented in this study should be confronted with field data. Additional thermokinetic tests for waste rock samples are required in order to provide reliable entry data for future predictive waste rock models. The effects of convective oxygen transport and water transport on the critical values of the dimensionless scaling parameter should be analyzed in a future study.

Usual acid/base accounting tests do not provide data necessary for a predictive model which should generate quantitative information about the effluent. Additional *thermokinetic* tests are proposed in order to provide experimental information necessary for a predictive waste rock model.

We hope that after further modifications and calibration, the scaling analysis presented here may help to properly design and manage waste rock piles and dumps.

## RÉSUMÉ

La nature particulièrement non linéaire des équations cinétiques décrivant les processus géochimiques et physiques agissant ensemble dans l'oxydation de la pyrite a soulevé des questions importantes sur la prévisibilité des répercussions sur l'environnement du drainage des eaux acides provenant des stériles. En réponse à ces questions, le présent rapport décrit les résultats d'un projet de recherche qui a été amorcé dans le but d'analyser quantitativement les processus chimiques et physiques élémentaires combinés qui sont à l'origine de l'oxydation de la pyrite et de l'acidification des eaux de drainage des stériles. Ce projet fait partie de mesures prises pour concevoir des indicateurs pratiques qui combineraient les données quantitatives de laboratoire, obtenues de petits échantillons de stériles, dont les effets observés dans les haldes de stériles sont à grande échelle.

Le principal objectif du présent projet était de déterminer les simples lois d'échelle qui gouvernent le comportement géochimique et thermodynamique de la roche pyritique dans les haldes de stériles. L'indicateur d'échelle $\delta$ qui combine les informations sur les processus se produisant à différentes échelles, est un élément innovateur du projet.

Les équations cinétiques effectives des réactions chimiques couplées se produisant pendant l'oxydation de la pyrite ont été établies. La concentration d'oxygène dissous a été décrite par une simple formule qui corrobore quantitativement les données expérimentales pour tout l'intervalle des températures et des concentrations de l'oxygène dans la phase gazeuse, tel qu'exigé pour l'analyse du drainage des eaux acides provenant de stériles. La forte diminution de la concentration de l'oxygène dissous avec la température est incluse dans le modèle. Elle ne l'avait pas été dans les modèles antérieurs - ce qui a pu causer une surestimation du potentiel d'acidification.

L'énergie et le transport de l'oxygène sont décrits en utilisant un modèle de réaction-transport. La forte dépendance non linéaire des vitesses de réaction effectives sur les paramètres physiques, minéralogiques et chimiques a été décrite au moyen d'un paramètre d'échelle $\delta$ que l'on peut utiliser comme indicateur pratique de drainage d'eaux acides provenant de haldes de stériles. Le paramètre d'échelle sans dimension $\delta$ combine des informations sur la porosité de la halde, la taille de la halde, la superficie de réaction effective, l'effet de la température sur la vitesse d'oxydation de la pyrite, la diffusion de l'oxygène dans la phase gazeuse, la chaleur de réaction de l'oxydation de la pyrite, la conductivité thermique des stériles et la température ambiante.

L'analyse de la sensibilité fournit des informations sur la précision requise pour les essais expérimentaux et l'importance relative des paramètres agissant sur les différents processus physiques et géochimiques à l'origine des eaux acides provenant de haldes de stériles. En particulier, il est montré que l'efficacité des couvertures imperméables s'accroît avec la concentration de la pyrite.

L'analyse d'échelle indique que les processus géochimiques et de transport fonctionnent à l'échelle moyenne d'une façon fondamentalement différente de l'échelle réelle. Les valeurs critiques du paramètre d'échelle $\delta$ auxquelles ont lieu des bifurcations ou des *catastrophes thermodynamiques* aboutissant à une accélération de l'acidification, ont été déterminées dans différents scénarios. Le fait crucial que l'acidification des eaux drainant les haldes de stériles dépend de la porosité des haldes, de la taille des haldes et de leur surface de réaction est l'une des

conclusions de l'analyse de bifurcation. Les résultats de l'analyse d'échelle offrent la possibilité d'une évaluation provisoire rapide et peu coûteuse des répercussions prévues sur l'environnement.

Tous les paramètres et toutes les variables du présent modèle peuvent être mesurés dans des expériences indépendantes. Le modèle produit des résultats réalistes en ce qui concerne les vitesses d'acidification sans l'introduction de paramètres ajustables utilisés par tous (connus de nous) les autres modèles de stériles. Plusieurs résultats de la présente étude diffèrent considérablement des conclusions et des hypothèses d'autres modèles.

Les résultats quantitatifs présentés dans l'étude devraient être confrontés aux données recueillies sur le terrain. Des essais thermocinétiques additionnels sur des échantillons de roches de stériles doivent être réalisés pour obtenir des données d'entrée fiables pour les modèles prédictifs futurs de stériles. Les effets du transport de l'oxygène par convection et du transport de l'eau sur les valeurs critiques du paramètre d'échelle sans dimension devraient être analysés dans une étude future.

Les essais habituels pour déterminer l'équilibre acide-base ne permettent pas de concevoir un modèle prédictif qui produirait des informations quantitatives sur les effluents. Pour obtenir les informations expérimentales nécessaires à un modèle prédictif des stériles, il est proposé de réaliser des essais *thermocinétiques* additionnels.

Nous espérons qu'après d'autres modifications et étalonnages, l'analyse d'échelle présentée facilitera la conception et la gestion des haldes de stériles.

## 1.0 INTRODUCTION

The purpose of this project is to provide a simple quantitative description of the interrelated nonlinear physical and chemical processes responsible for ARD. Accurate prediction and understanding of acid rock drainage may be based on the analysis of quantitative data from experiments and physico-chemical models, and potentially offers a cost-effective means of reducing the environmental impact of ARD.

It is believed that practical decisions should be based on the quantitative results of laboratory and field tests. Laboratory tests analyze various aspects of acid rock drainage by using a limited amount of waste rock, ranging from one to a thousand kilograms (meso-scale). Such tests concentrate on characterization of the chemical properties of waste rock. Because the processes involved are nonlinear, scaling up the meso-scale results to obtain macro-scale characteristics for millions of tons of waste rock is a difficult task which requires an extensive modelling effort. Tests for ARD prediction (e.g. humidity cells, column tests, small scale treatment systems) are used frequently to determine the optimum approach to minimizing the environmental impact and treatment cost. No researcher, however, has examined the size effects that may be significant for the prediction of macro-scale behaviour. Such efforts are often hindered by the long computation time required for parametric analysis of numerical models. Finding the appropriate scaling relations between physical, chemical and biological processes is one of the goals of this study. Knowledge of the scaling laws may allow one to improve interpretation of the existing experimental data, design better micro-scale and meso-scale experiments and reduce the cost of prediction techniques by using cheaper small scale experiments.

Prediction of long term environmental impact, based on the characterization of waste materials is not a simple task, however. Apart from chemical processes, ARD depends also on physical, biological and mineralogical factors. Chemical and biological aspects of acidic drainage were analyzed in our recent study [SyT]. It has been found that the interrelated elementary chemical and microbial reactions have to be described as coupled nonlinear processes which respond in a rather complex way to preventive measures like neutralization and oxygen depletion. Temperature is a very important factor. The rates of oxygen and water transport also are important factors to consider due to their effect on both oxidation and heat exchange with the surroundings.

Extensive computer models which have to be analyzed numerically, often require a very long computational time before one is able to gather quantitative information about the complexity of the coupled physical and chemical processes. Scaling relations based on the consideration of simplified reaction transport models often give good quantitative information about the relative importance of the factors involved, and allow one to translate laboratory data into large-scale estimates.

In this report we concentrate on the interplay between the chemical kinetics and transport of mass and energy. Mass and energy transport are physical factors which ultimately control reaction rates. The concentration of oxygen and the temperature distribution are non-homogeneous inside waste rock pile [PaR], [FeM], [BeR], [Ge], [NoD]. The quantitative analysis

of the expected distribution of oxygen and temperature is important for the estimation of acid generation.

Previous waste rock models did not describe properly the process of pyrite oxidation in regions where oxygen concentration is low and temperature is high. In particular, to our knowledge, the temperature dependence of oxygen dissolved in water has not been included in previous models. [BeR], [BrC], [CdO], [Da], [DaR1], [DaR2], [DaR3], [FeE1], [Ge], [Res], [WhJ].

The report starts with an analysis of a kinetic chemical model which lays the ground for the quantitative physico-chemical model. In Chapter 2, we analyze the following coupled processes:

- pyrite oxidation by water and oxygen dissolved in water and the release of $Fe^{2+}$ (ferrous) ions and acid (reaction (R1))
- oxidation of ferrous ions to ferric ($Fe^{3+}$) ions by oxygen (reaction (R2))
- anaerobic oxidation of pyrite by ferric ions and water (reaction (R3))
- precipitation of ferric hydroxide, which eliminates ferric ions from the stream (reaction (R4))
- the neutralization process

Effective kinetic models for chemical reactions at high and low pH values are constructed and analyzed in Chapter 3. The temporal behaviour of the concentrations of chemical species is considered separately for pH values greater than four, and less than four. This distinction is necessary because of the dramatic changes in the nature of pyrite oxidation due to the precipitation of ferric hydroxide at pH values above four. Pyrite oxidation rates increase dramatically with temperature - for temperatures between 273K and 323K the rate of pyrite oxidation accelerates about ten times per 20K. Transport processes which control the supply of water and oxygen, are ultimately responsible for both the rate of acid generation and its release to the environment. The form of the effective kinetic equations derived in Chapter 3 is suitable for the scaling analysis of the reaction-diffusion equations in Chapter 4.

In Chapter 4 the mathematical scaling analysis of coupled chemical and physical processes is presented. We derive a dimensionless physico-chemical scaling parameter, $\delta$, which describes the combined effects of chemical reactions and mass and energy transport. The dimensionless scaling parameter $\delta$ describes the relative effects of oxygen diffusion, thermal conductivity, pile porosity, ambient conditions, etc. The relative importance of the different factors involved in acid rock drainage is described quantitatively by the dimensionless scaling parameter which may become useful as a standard tool for predictive analysis of laboratory and field data. The strongly nonlinear properties of the combined physical and chemical processes are analyzed as a function of the parameters describing pile size, pile porosity, pyrite content and other quantities. It is found that there exist *critical* values of these parameters at which a discontinuous increase of chemical rates may take place together with a jump-wise increase of temperature and acid generation rates inside waste rock piles. We call this phenomenon a *thermodynamic catastrophe*. This aspect of ARD is very important for the prediction and control of acid rock drainage and to the best of our knowledge has not been discussed in previous studies.

In Chapter 5, different scenarios of acid generation for different sets of input data are analyzed in detail. The power of scaling analysis is demonstrated by showing how the results for

one set of entry data can be obtained from results derived for a different set of entry data. Maximum allowed values of pile size and effective reactive surface area are calculated for two different realistic scenarios of ARD. Also, in Chapter 5, the required accuracy of experimental tests is analyzed.

The dimensionless scaling parameter, $\delta$, presented in this report is more general and provides more information than the Thiele modulus typically used in literature [Ar], [DrA]. The scaling analysis has been performed by analytical mathematical methods with a minimum use of numerical analysis. In the next step, the results presented in this report should be confronted with available experimental data on acid drainage. Data collected during field tests and laboratory thermokinetic experiments involving large samples of pyritic rocks should be used to calibrate the model.

## 2.0 OXIDATION OF PYRITE

In this Chapter, the complex kinetics of pyrite oxidation is briefly summarized. We refer the reader to [SyT] and references therein for more details and further references.

The overall stoichiometry of pyrite oxidation may be described by the following reactions:

$$FeS_2 + 7/2\ O_2 + H_2O = Fe^{2+} + 2\ SO_4^{2-} + 2H^+, \qquad (S1)$$

$$FeS_2(s) + 15/4\ O_2\ (aq) + 7/2\ H_2O = Fe(OH)_3(s) + 4H^+ + 2SO_4^{2-} \qquad (S2)$$

Reactions (S1) and (S2) summarize several elementary chemical reactions which take place at low pH values (reaction (S1)) or high pH values (reaction (S2)).

In order to describe the oxidation kinetics, the intermediate steps in this reaction must be considered. The following reactions characterizing the oxidation of pyrite have been proposed [StM], [SiS], [TaW]:

$$FeS_2(s) + 7/2\ O_2 + H_2O = Fe^{2+} + 2SO_4^{2-} + 2H^+ \qquad (R1)$$

$$Fe^{2+} + 1/4\ O_2 + H^+ = Fe^{3+} + 1/2\ H_2O \qquad (R2)$$

$$FeS_2(s) + 14Fe^{3+} + 8H_2O = 15Fe^{2+} + 2SO_4^{2-} + 16H^+ \qquad (R3)$$

$$Fe^{3+} + 3H_2O = Fe(OH)_3(s) + 3H^+ \qquad (R4)$$

The chemical network responsible for pyrite oxidation consists of four reactions:

(R1) The oxidation of pyrite by molecular oxygen to $Fe^{2+}$ and sulphate. The oxidation of iron sulphide (pyrite) to sulphate (eq. (R1)) releases dissolved ferrous ions and acidity into the water.

(R2) Subsequently, the dissolved ferrous ions undergo oxidation to ferric ions (eq. (R2)). This is a slow reaction and viewed as the rate-limiting step determining the overall rate of pyrite oxidation.

(R3) Sulphide is oxidized again by ferric ion and acidity is released along with additional ferrous ions which may re-enter the reaction cycle via reaction (R2). This is regarded as a fast step.

(R4) Ferric ions hydrolyse to form insoluble ferric hydroxide (eq. (R3)), releasing more acidity to the stream. This reaction takes place only at high pH values which can be attained when the mineral composition of the waste rock is such that self-buffering processes take place or when neutralizing minerals are added.

Reactions (R2) and (R3) provide a feedback loop discussed by Singer and Stumm (p. 471 of ref. [StM]). Ferrous iron produced in (R3) is utilized again in reaction (R2).

The number of reacting species during acid formation is greater than two. This leads to strong nonlinearities in the kinetic equations.

### 2.1 Oxidation at pH Between 4 and 7

The set of coupled kinetic differential equations has been derived in our previous study and has the form:

$$\frac{d[Fe^{2+}]}{dt} = \frac{S}{V} k_1(T)[O_2]^{1/2} k_2(T,[H^+])[Fe^{2+}][O_2] \qquad (D1.1)$$

$$\frac{d[Fe(OH)_3]}{dt} = k_2(T,[H^+])[Fe^{2+}][O_2] \qquad (D1.2)$$

$$\frac{d[H_2O]}{dt} = \frac{S}{V} k_1(T)[O_2]^{1/2} \frac{5}{2} k_2(T,[H^+])[Fe^{2+}][O_2] \qquad (D1.3)$$

$$\frac{d[O_2]}{dt} = \frac{7S}{2V} k_1(T)[O_2]^{1/2} \frac{1}{4} k_2(T,[H^+])[Fe^{2+}][O_2] \qquad (D1.4)$$

$$\frac{d[SO_4^{2}]}{dt} = \frac{2S}{V} k_1(T)[O_2]^{1/2} \qquad (D1.5)$$

$$\frac{d[H^+]}{dt} = \frac{2S}{V} k_1(T)[O_2]^{1/2} + 2\,k_2(T,[H^+])[Fe^{2+}][O_2] \qquad (D1.6)$$

In our previous study we have presented numerical solutions to the set of equations (D1) for the experimentally determined values of the temperature and pH dependent rate constants k(T) and reactive surface area, S per unit volume, V.

## 2.2 Oxidation at pH Less Than 4

At low pH values ferric hydroxide does not precipitate if concentrations of ferric iron are sufficiently small. This means that the ferric iron, $Fe^{3+}$ (which is formed by oxidation of ferrous iron) oxidizes pyrite according to the reaction (R3). The set of coupled kinetic differential equations has the form:

$$\frac{d[Fe^{2+}]}{dt} = \frac{S}{V} k_1(T)[O_2]^{1/2} k_2(T,[H^+])[Fe^{2+}][O_2] + \frac{15S}{14V} k_3[Fe^{3+}]^{3/5}[H^+]^{1/2} \qquad (D2.1)$$

$$\frac{d[Fe^{3+}]}{dt} = k_2(T,[H^+])[Fe^{2+}][O_2] \frac{S}{V} k_3(T)[Fe^{3+}]^{3/5}[H^+]^{1/2} \qquad (D2.2)$$

$$\frac{d[H^+]}{dt} = \frac{2S}{V} k_1(T)[O_2]^{1/2} k_2(T,[H^+])[Fe^{2+}][O_2] + \frac{8S}{7V} k_3(T)[Fe^{3+}]^{3/5}[H^+]^{1/2} \qquad (D2.3)$$

$$\frac{d[O_2]}{dt} = \frac{7S}{2V} k_1(T)[O_2]^{1/2} \frac{1}{4} k_2(T,[H^+])[Fe^{2+}][O_2] \qquad (D2.4)$$

$$\frac{d[SO_4^2]}{dt} = 2\, k_1(T)[O_2]^{1/2} + \frac{S}{7V} k_3(T)[Fe^{3+}]^{3/5}[H^+]^{1/2} \qquad (D2.5)$$

$$\frac{d[H_2O]}{dt} = \frac{S}{V} k_1(T)[O_2]^{1/2} + \frac{1}{2} k_2(T,[H^+])[Fe^{2+}][O_2] \frac{4S}{7V} k_3(T)[Fe^{3+}]^{3/5}[H^+]^{1/2} \qquad (D2.6)$$

The use of the full set of the kinetic equations in a physicochemical model is not practical, however, because of the required long computer time when transport processes are included. The main factors affecting the rates of acid production are concentration of oxygen, temperature and pH value. Because in our previous study no oscillatory or chaotic behaviour of the coupled chemical equations (D1) and (D2) has been found, the detailed kinetic equations can be replaced by much simpler effective equations suitable for the physico-chemical model. The most significant information can be obtained by analyzing the temperature dependence of the overall rates of oxygen consumption and the dependence of acid production rates on temperature. We have analyzed our previous numerical results and on that basis it is possible to derive effective kinetic equations for oxygen. The effective kinetic equations are subsequently used as a starting point for the scaling analysis. Numerical solutions to the kinetic equations (D1) and (D2) are presented in Appendix A. The previous report [SyT] discusses the agreement of the results obtained for the kinetic equations with laboratory data.

## 3.0 EFFECTIVE KINETIC EQUATIONS FOR THE OXIDATION OF PYRITE

This Chapter presents the results of our mathematical analysis of numerical results obtained for a set of kinetic equations discussed in Chapter 2. The purpose of our analysis is to derive closed form formulae for overall oxygen consumption rates and thermal energy generation rates. The effective formulae have a simple form suitable for the scaling analysis of coupled physical and chemical processes.

The scaling parameters discussed in this Chapter allow the estimation of the temperature dependent rates for processes contributing to acid rock drainage, without solving the differential equations.

In Sections 3.1 and 3.2 we analyze two aspects of pyrite oxidation:

i) Scaling relations determined by the quantitative analysis of the chemical reactions described in the previous section; and

ii) Scaling relations for the concentration of oxygen dissolved in water as a function of temperature and concentration of oxygen in the gas phase.

In Section 3.3 effective equations for oxygen consumption rates and energy generation rates are derived for different pH values.

### 3.1 Scaling Relations for Chemical Reactions

The scaling parameters should be useful for analyzing certain site-specific situations where values for material parameters and initial conditions are different than the particular values used in this report. The scaling analysis for chemical rates will be used subsequently in our bifurcation analysis of the reaction-transport scaling model which will include processes of mass and energy transport.

There is one obvious scaling parameter, S/V, which relates time scales of the surface reactions (R1) and (R3) to the active surface area and water volume. We can also define other scaling factors which relate quantities characterizing acidic drainage for different conditions labelled byi and j.

For the reaction (R1) we define the scaling factors:

$$r_1(i,j) = \frac{S_i / V_i}{S_j / V_j} \frac{[O_2(t_o)]_i^{1/2}}{[O_2(t_o)]_j^{1/2}} \qquad (3.1)$$

and

$$f_1(T_o, \Delta T) = \exp\left[\frac{E_1}{R(T_o + \Delta T)}\right] / \exp\left[\frac{E_1}{R T_o}\right] \qquad (3.2)$$

The thermodynamic scaling factor $f_1(T_o,\Delta T)$ tells us that when we increase temperature by $\Delta T$, the rate constant will change $f_1(T_o,\Delta T)$ times. The thermodynamic scaling factors satisfy a recursion relation:

$$f_1(T_o, 2\Delta T) = f_1(T_o, \Delta T)\, f_1(T_o + \Delta T, \Delta T) \qquad (3.3)$$

It turns out that for activation energy values on the order of $10^5$J and temperatures between $T_{min}$=283 K and $T_{max}$=333 K the scaling factor defined by eq.(3.2), can be approximated by the factor $f_1(\Delta T)$ which does not depend on $T_o$. At first we find the ratio between the greatest and the smallest values of the rate constant $k_1(T)$:

$$f_1(T_{max}\, T_{min}) = \exp[\frac{E_1}{R\,T_{max}}] / \exp[\frac{E_1}{R\,T_{min}}] \qquad (3.4)$$

Then the thermodynamic scaling factor $f_1(\Delta T)$ is defined as:

$$f_1(\Delta T) = \{ f_1(T_{max}\, T_{min}) \}^{\Delta T/(T_{max} T_{min})} \qquad (3.5)$$

which satisfies a recursion relation:

$$f_1(n\Delta T) = [\, f_1(\Delta T)\,]^n \qquad (3.6)$$

The accuracy of the approximation $f_1(\Delta T) \approx f_1(T_o, \Delta T)$ is better than 10%. Subscripts *l* and *h* label results obtained for low (at pH<4) and high pH values respectively. For the reaction (R1) at pH<4, when $E_{1l}$=57 kJ/mol, we obtain:

$$f_{1l}(\Delta T = 10K) = 2.1 \qquad (3.7)$$

which means that if we increase the temperature by 10K, then the rate constant for the oxidation by dissolved oxygen increases 2.1 times. For high pH values, when $E_{1h}$=88 kJ/mol we obtain:

$$f_{1h}(\Delta T = 10K) = 3.1 \qquad (3.8)$$

We may combine factors $r_1$ and $f_1$ and define the scaling factor:

$$F_1 = r_1\, f_1 \qquad (3.9)$$

which takes into account the effective active surface area, the amount of water, oxygen concentration and temperature. We can use the scaling factor $F_1$ to transform the results obtained for one set of material parameters and initial conditions into results for different values of parameters and initial conditions. The conclusions are based on our analysis of experimental data and numerical results presented in [SyT] (See Appendix A and Appendix B). For example, by comparing Figs. A3(21) and A.3(31) we see that Fig. A3(21) can be obtained from Fig. A3(31) after rescaling the time axis by the factor $F_1(\Delta T=20K)$ equal to 8.2 (calculated by using the eqs. (3.1), (3.8) and (3.9) and taking into account the decreasing concentration of dissolved oxygen - see Table 3.1 on p. 17).

In a similar way we may derive scaling factors $f_2$ and $f_3$ for the reactions (R2) and (R3). At low pH values we can use the average activation energy $(E_{2l}+E_{2l})/2$ to define:

$$f_{2l}(\Delta T = 10K) = 2.9 \qquad (3.10)$$

For the reaction (R3) (for which the activation energy $E_3$=90 kJ/mol [MaR2], [WiR]) we obtain:

$$f_3(\Delta T = 10K) = 3.3 \qquad (3.11)$$

For ΔT=20 K the thermodynamic scaling factor $f_3$(20K)=10.7. Fig. 3.1 presents numerical solutions to eqs. (D2) for large initial values of $[Fe^{3+}]$ at different temperatures and for different values of S/V.

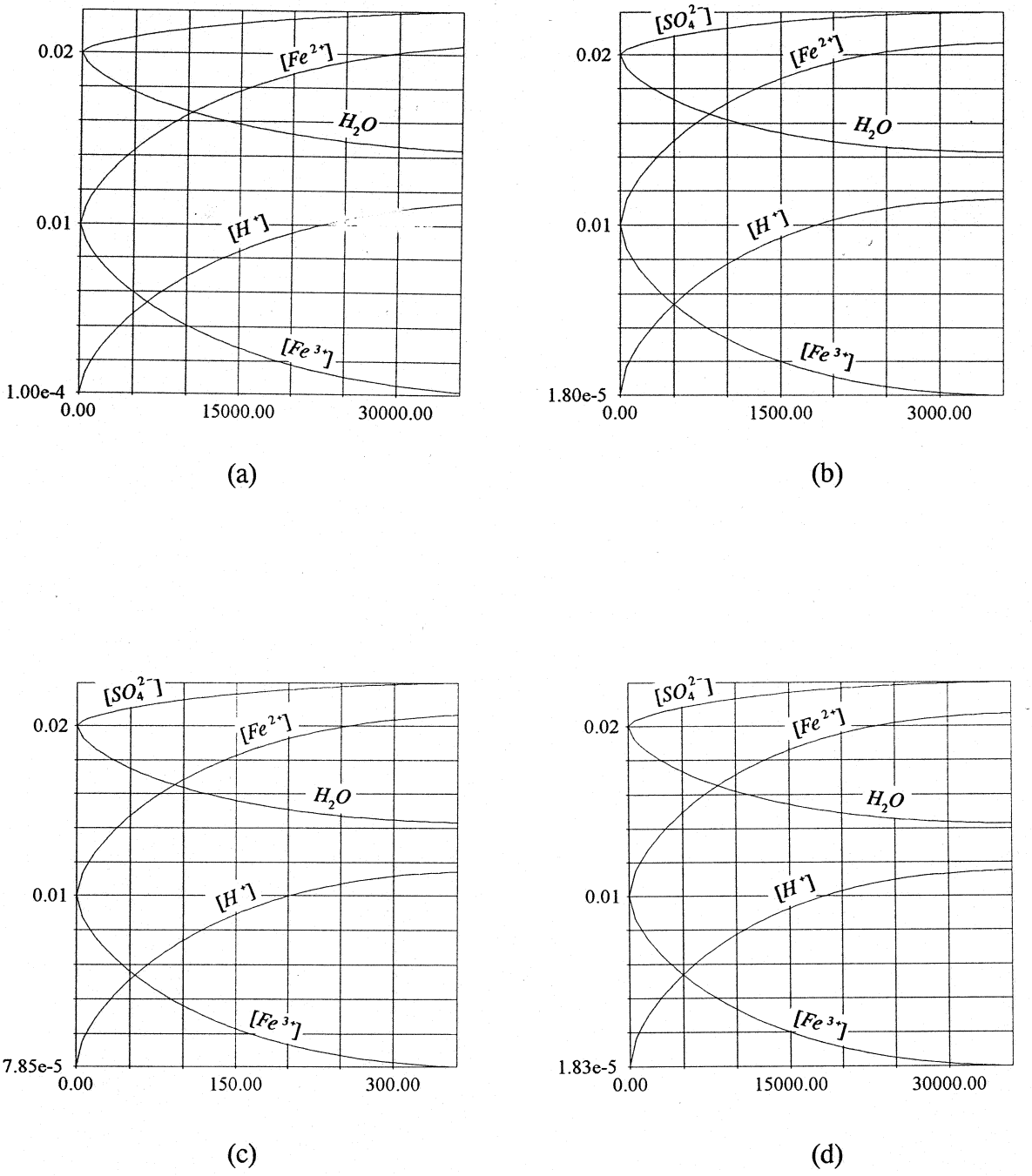


Fig. 3.1 Numerical solutions to eqs.(D2) for the initial values $[Fe^{2+}(t_o)]=Fe^{3+}(t_o)]=0.01M$, $[H^+(t_o)]=10^{-4}M$. Plots (a), (b) and (c) obtained for $S/V=1m^2/l$ and temperatures 283K, 303K and 323K respectively; (d) obtained for $S/V=10m^2$ and T=303 K. Vertical axis: molar concentrations; horizontal axis: time in seconds (30 000 s = 8 hours).

As we see, Figures 3.1 (a) and 3.1 (d) are almost identical. They are related by the scaling factor $F_3=f_3(20K)S(d)/S(a)=1.07$. Figs. 3.1 (a), (b) and (c) are related by the scaling factor $f_3(20K)=10.7$.

More complex symmetries of differential equations and more complicated scaling relations will be used in Chapter 4 to analyze reaction-transport models defined by coupled partial differential equations [Ar], [BaZ]. In our further analysis we follow principles used for other known examples of reaction-transport problems for which the scaling relations allow the determination of a bifurcation structure and reduce computation time [Ar], [Ot], [SyT]. The results of this report can be used as a starting point for analyzing the scaling properties of a waste rock model or a model for underwater disposal.

## 3.2 Scaling Formula for Concentration of Oxygen Dissolved in Water

Table 3.1 presents data on the concentrations of oxygen dissolved in water, $[O_2]$ (in units of mol per litre) as a function of the temperature and oxygen concentration in the gas phase, $[O_2]_{gas}$ (in volume %). The temperature values correspond to those observed in waste rock piles. $[O_2]$ increases slightly faster than linearly with $[O_2]_{gas}$ at constant temperature. At $50^oC$ and $[O_2]_{gas}=21\%$, $[O_2]$ is less than 50% of its value at $10^oC$. In this way we observe a competitive effect of temperature and dissolved oxygen concentration on the reaction rates.

The values in Table 3.1 are obtained for water without any dissolved iron or sulphate ions. Unfortunately we do not have any experimental data on the concentrations of dissolved oxygen in the presence of iron and sulphate ions at various pH values. We will simply assume that the maximum concentration of oxygen dissolved in water does not depend on pH. This assumption is supported by the fact that the order of reaction (R3) with respect to oxygen does not depend on pH, as discussed by McKibben and Barnes [McK].

The solubility of oxygen in water can be described by the relation:

$$[O_2]_w = 100\,mmol/l\left(\frac{[O_2]}{10\%}\right)^{1.2}\left(\frac{30^oC}{T}\right)^{0.5} \qquad (3.12)$$

The last formula gives the values of concentration of dissolved oxygen in water in micromoles of oxygen per litre when concentration of oxygen in the gas phase is measured as a percentage of the total volume of air and temperature is measured in $^oC$. This formula gives better than 10% average agreement with the experimental data presented in Table 3.1.

Eq. (3.12) introduces the temperature dependent factor which inhibits oxidation rates at high temperatures. To our knowledge, this effect has not been analyzed in previous models for acid rock drainage.

In Chapters 4 and 5 we will use the variable Y which will denote $[O_2]_{gas}$ expressed in units of mol per cubic meter and appropriately transformed formula (3.12) will be used.

| T °C | $[O_2]_{gas}$=21% | | $[O_2]_{gas}$=15% | | $[O_2]_{gas}$=10% | | $[O_2]_{gas}$=5% | | $[O_2]_{gas}$=1% | |
|---|---|---|---|---|---|---|---|---|---|---|
| | mg | µmol | mg | µmol | mg | µmol | mg | µmol | mg | µmol |
| 5 | 12.79 | 399.6 | 9.60 | 299.9 | 6.02 | 188.1 | 2.92 | 91.2 | 0.50 | 15.6 |
| 10 | 11.30 | 353.0 | 8.03 | 250.9 | 5.31 | 165.9 | 2.59 | 80.9 | 0.41 | 12.8 |
| 15 | 10.11 | 315.9 | 7.16 | 223.7 | 4.72 | 147.5 | 2.27 | 70.9 | 0.32 | 10.0 |
| 20 | 9.12 | 284.9 | 6.45 | 201.5 | 4.23 | 132.2 | 2.01 | 62.8 | 0.23 | 7.2 |
| 25 | 8.30 | 259.3 | 5.86 | 183.1 | 3.77 | 117.8 | 1.82 | 56.8 | 0.14 | 4.4 |
| 30 | 7.60 | 237.5 | 5.33 | 166.5 | 3.44 | 107.5 | 1.56 | 48.7 | 0.05 | 1.6 |
| 35 | 7.00 | 218.7 | 4.88 | 152.5 | 3.12 | 97.5 | 1.43 | 44.7 | 0.00 | 0.0 |
| 40 | 6.47 | 202.1 | 4.47 | 139.7 | 2.81 | 87.8 | 1.15 | 35.9 | 0.00 | 0.0 |
| 45 | 6.00 | 187.5 | 4.10 | 128.1 | 2.52 | 78.7 | 0.94 | 29.4 | 0.00 | 0.0 |
| 50 | 5.57 | 174.0 | 3.75 | 117.2 | 2.25 | 70.3 | 0.74 | 23.1 | 0.00 | 0.0 |
| 55 | 5.17 | 161.5 | 3.55 | 110.9 | 1.96 | 61.2 | 0.50 | 15.6 | 0.00 | 0.0 |
| 60 | 4.89 | 152.8 | 3.38 | 105.6 | 1.64 | 51.2 | 0.25 | 7.8 | 0.00 | 0.0 |

Table 3.1 Saturation concentrations of dissolved oxygen in water, $[O_2]$ , at atmospheric pressure (1013.25 hPa) for different oxygen concentrations in the gaseous phase $[O_2]_{gas}$. The solubilities of oxygen are defined in terms of the mass of oxygen dissolved in one litre of the water in equilibrium with an atmosphere saturated with water vapour at various temperatures. The data are calculated following Benson and Krause [BeK] and using a computer program published by Beer [Be].

### 3.3 Effective Kinetic Equations

Rates of oxygen consumption and energy release can be derived as effective rates taking into consideration the summary effect of all reactions involved. Our quantitative analysis of experimental data and numerical analysis of eqs. (D1) and (D2) issummarized below.

#### *3.3.1. pH between 4 and 7*

1) The acid production rates are directly proportional to the coefficient S/V which measures the ratio between the active surface area of pyritic rock per volume of water.
2) Oxygen consumption rates increase at the rate of 3.1 times per 10K. This corresponds to the power law increase $T^{3.30}$ with temperature T measured in $^{o}$C. This formula gives better than 5% agreement with both laboratory data and our previous numerical results over the temperature range from 0$^{o}$C to 60$^{o}$C typical for waste rock piles.
3) The total rate of iron production (as $Fe^{2+}$ and $Fe(OH)_3$ ) is proportional to the rate of oxygen consumption with the molar proportionality coefficient (0.28±0.01) in the temperature range between 0$^{o}$C and 60$^{o}$C (see Figs. A1 and A2).
4) The rate of sulphate ion production follows the stoichiometry of the reactions (R1)-(R4) and is twice as high as that of the ferrous iron production. The molar coefficient with respect to oxygen is 0.56±02 (i.e. 0.56mol of sulphate produced per 1mol of oxygen consumed).
5) The solubility of oxygen in water can be described by the relation (µmol/l of oxygen in water)=100 µmol/l $\{[O_2]_{gas}/(10\%)\}^{1.2}(30^{o}C/T)^{0.5}$ which describes the dependence of dissolved oxygen as a function of temperature and oxygen concentration in the gas phase.

Based on the results summarized above the effective kinetic equations for oxygen consumption and energy release have the form:

$$\frac{d[O_2]}{dt} = k_h \frac{S}{V} [O_2]^{0.6} T^{3.3} \qquad (3.13)$$

$$\frac{dQ}{dt} = h\, k_h \frac{S}{V} [O_2]^{0.6} T^{3.3} \qquad (3.14)$$

where h is the heat of pyrite oxidation permol of oxygen consumed.

### *3.3.2 pH Less Than 4*

1) The acid production rates are directly proportional to the coefficient S/V which measures the ratio between the active surface area of pyritic rock per volume of water.
2) Oxygen consumption rates increase at the rate of 2.5 times per 10K. This corresponds to the power law increase $T^{2.6}$ with temperature T.
3) The rate of ferrous iron production is proportional to the rate of oxygen consumption with the molar proportionality coefficient (0.29±0.01) in the temperature range between 0°C and 60°C.
4) The rate of sulphate ion production follows the stoichiometry of the reactions (R1)-(R4) and is twice as high as that of the ferrous iron production. The molar coefficient with respect to oxygen is 0.58±02 (i.e. 0.58 mol of sulphate produced per 1 mol of oxygen consumed).
5) The solubility of oxygen in water can be described by the relation (µmol/l of oxygen in water) = 100 µmol $\{[O_2]_{gas}/(10\%)\}^{1.2}(30^oC/T)^{0.5}$ which describes the dependence of dissolved oxygen as a function of temperature and oxygen concentration in the gas phase.

The molar coefficients are significantly affected by the bacterial oxidation. (See ref. [SyT] for details).

The kinetic equations have the form:

$$\frac{d[O_2]}{dt} = k_I \frac{S}{V} [O_2]^{0.6} T^{2.6} \qquad (3.15)$$

$$\frac{dQ}{dt} = h\, k_I \frac{S}{V} [O_2]^{0.6} T^{2.6} \qquad (3.16)$$

In Chapter 4 the rate equations (3.13)-(3.16) will be used in the reaction-transport scaling model. The effective kinetic equations derived in this Chapter are based on laboratory data obtained for small samples of pyrite in water. In our further analysis we replace the coefficient kS/V by the coefficient *a*S in which S is the reactive surface area of pyrite in one cubic meter of waste rock and *a* is the rate constant in the appropriate units (see Tables 5.1 and 5.2).

## 4.0 SCALING ANALYSISOF COUPLING BETWEEN CHEMICAL KINETICS AND TRANSPORT PHENOMENA

Mass and energy transport can be modelled by nonlinear partial differential equations which describe the spatially nonhomogeneous distribution of oxygen, water, reaction products and temperature as a function of physical and mineralogical properties such as pile porosity, oxygen transport rate, thermal conductivity, etc. [cD], [Sch], [Ar], [Ot1], [Ot2].

In this Chapter, multiple steady state solutions are calculated exactly and the bifurcation diagram is analyzed. The scaling analysis is performed in order to establish the relative importance of individual factors responsible for acid rock drainage. The relative importance of various physical and chemical factors responsible for acid rock drainage is described by means of a dimensionless scaling parameter $\delta$ which contains quantitative information about the different processes involved. The scaling model covers a broad range of chemical and physical parameters.

Long term predictions can be usually based on quantitative results obtained for steady state solutions of reaction-transport models. One has to remember, however, that rock texture undergoes changes during weathering processes, and parameters such as the reactive surface area change over time. To our knowledge, the only detailed study of temporal changes in the reactive surface area has been performed for tailings [Ni], [NiG]. A similar long term study for waste rock would provide useful information for the present scaling analysis. Because of the lack of quantitative experimental data we do not attempt to model temporal changes in the reactive surface area, S.

### 4.1 Formulation of the Reaction-Transport Model

From a physico-chemical point of view a pile of waste rock reacting with oxygen and water is an open non-equilibrium system evolving towards an equilibrium state in which pyrite is transformed into ferrous/ferric iron and acid.

The overall process of pyrite oxidation in waste rock piles can be described by a set of two coupled nonlinear parabolic equations in two fields, oxygen concentration, Y and temperature, T:

$$[e\, r_a C_a + (1e)\, r_r C_r]\frac{\partial T}{\partial t} = l\,\frac{\partial^2 T}{\partial x^2} + h(1e)aS\,T^q Y^p \qquad (4.1)$$

$$e\frac{\partial Y}{\partial t} = eD\frac{\partial^2 Y}{\partial x^2}(1e)aS\,T^q Y^p \qquad (4.2)$$

Equations (4.1) and (4.2) are the energy and mass conservation equations, respectively. (T - temperature, Y - oxygen concentration in the gas phase, $\varepsilon$ - porosity of the pile, $\rho_a$ - air density, $C_a$ - specific heat of air, $\rho_r$ - rock density, $C_r$ - specific heat of rock, $\lambda$ - thermal conductivity of the pile (air+rock), h - heat of reaction of oxygen with pyrite, D - diffusion coefficient of oxygen in the gas phase, q - effective thermal exponent, p - effective order of chemical reaction of oxygen with pyrite.)

The values of *a*, p and q are different for different pH values. For pH less than 4 p=0.6, q=2.1. For pH greater than 4, p=0.6, q=2.8. In order to simplify the scaling analysis we will use the value of p=1. We plan to properly calibrate our results when the results of thermokinetic tests at different values of oxygen partial pressure become available for rock samples.

We consider a pile characterized by the linear dimension L, with the oxygen concentration $Y_b$ at the boundaries, and temperature $T_b$ at the boundaries. For symmetric boundary conditions, for a steady state we have:

$$Y = Y_b k(T T_b); k = l(heD)^1 \qquad (4.3)$$

(For nonsymmetric boundary conditions

$$Y = Y_b - \kappa(T-T_b) - Cx \qquad (4.3a)$$

where C is a constant depending on the boundary conditions).

From equations (4.1) and (4.2) one obtains for steady state solutions:

$$\frac{\partial T}{\partial x} = +(A T^{q+2} B T^{q+1} + C)^{1/2} := [F(T;C)]^{1/2} \qquad (4.4)$$

where

$$A = \frac{2(1e)aS}{(q+2)eD]}, B = \frac{2aS(1e)}{De(q+1)}\left(\frac{Deh Y_b}{l} + T_b\right) \qquad (4.5)$$

The integration constant C is not a free parameter, but (for given values of parameters) is determined by $T_b$ and is implicitly related to L. For different values of C we obtain different values of the maximum temperature, $T_m$ in the pile. The linear size, L is given by the formula

$$L = 2\int_{T_b}^{T_m} [F(T;C)]^{1/2} dT \qquad (4.6)$$

Formula (4.6) defines implicitly the distribution of temperature T(x).

The maximum temperature in the pile cannot exceed the value:

$$T_m^* = T_b + l^1 heD Y_b \qquad (4.7)$$

At the point where the temperature $T_m^*$ is reached, the concentration of oxygen is equal to zero. Note that $T_m^*$ does not depend on the rate constant *a*S. Thus the state with zero oxygen concentration at the point of maximum temperature is controlled by oxygen transport.

In the next step we derive a dimensionless parameter δ which will define the scaling law involving all the parameters in equations (4.4) and (4.5).

We introduce the variables:

$$U = (A / B)T, r = C\, A^{q+1}\, B^{(q+2)} \qquad (4.8)$$

In terms of the new variables, the linear size can be expressed as an integral which depends only on the parameter r:

$$L = \frac{A^{(q1)/2}}{B^{q/2}} I[U_m; U_b] \qquad (4.9)$$

$$I[U_m; U_b] := \int_{U_b}^{U_m} [U^{q+2} U^{q+1} + r\,]^{1/2}\, dU \qquad (4.10)$$

The universal function $I[U_m; U_b]$ is presented in Figs. 4.2 and 4.3 for q=2.1 corresponding to low pH values and two different values of $U_b$ (see p. 27).

## 4.2 Scaling Properties and Sensitivity Analysis of Acid Rock Drainage

It is useful to define the dimensionless parameter:

$$d := L\frac{B^{q/2}}{A^{(q1)/2}} \qquad (4.11)$$

which after substituting expressions (4.5) defining the parameters A and B takes the form:

$$d := L\sqrt{\frac{2aS(1e)}{(q+2)De}}\left[\frac{q+2}{q+1}\left(\frac{DehY_b}{l}+T_b\right)\right]^{q/2} \qquad (4.12)$$

The scaling parameter δ is a combination of parameters describing physico-chemical properties of pyritic rock and storage conditions. The scaling parameter δ can be used as a quantitative indicator of acid rock drainage. Values of δ define different regimes of acid rock drainage. The greater the value of δ the greater the rate of acid generation. δ shows a strong nonlinear dependence on parameters characterizing acid rock drainage. Some of these parameters, like pile porosity and pile size, can be controlled. Maintaining the smallest possible value of δ is important in order to minimize the environmental impact of acid rock drainage. The expected environmental impact increases with the value of δ. (On the other hand, one may consider a controlled preemptive leaching over a short time in order to reduce the long term environmental impact and to increase production [Go]. In this scenario the large values of δ may be required in order to intensify leaching.)

The scaling indicator δ provides important quantitative information about relative importance of individual factors contributing to ARD. Because δ is proportional to $S^{1/2}$ the pile design parameters become increasingly important for large values of pyrite concentration. In particular, the effectiveness of impermeable covers increases with the pyrite concentration. In Chapter 5 we demonstrate how to use the scaling indicator δ for the predictive analysis of ARD.

The scaling formula (4.12) indicates the required precision of individual laboratory tests in which parameter values are determined. This aspect is analyzed in Section 5.4.

Laboratory tests usually measure acid generation over time and provide information about the chemical activity of pyritic rock (factor *a*S). Acid/base tests should also determine a detailed temperature dependence of acid generation rates at temperatures between $0^oC$ and $60^oC$. Experimental validation of the formula describing the dependence of reaction rates on oxygen concentration in the gas phase for different pH values also seems necessary. Such experimental tests would determine the values of parameters *a*, S and q which are crucial for reliable estimates based on the scaling parameter δ.

For given values of other parameters we obtain the condition:

$$L(1-\varepsilon)^{1/2}\varepsilon^{(q-1)/2} < \text{const.} \qquad (4.13)$$

which defines the optimum size of the pile as the function pile porosity, ε. The form of condition (4.13) indicates a very strong nonlinear dependence of acid rock drainage on ε. The porosity factor:

$$P(\varepsilon) = (1-\varepsilon)^{1/2}\varepsilon^{(q-1)/2} \qquad (4.14)$$

which enters the relation (4.14), affects very significantly the total rates of acid generation.

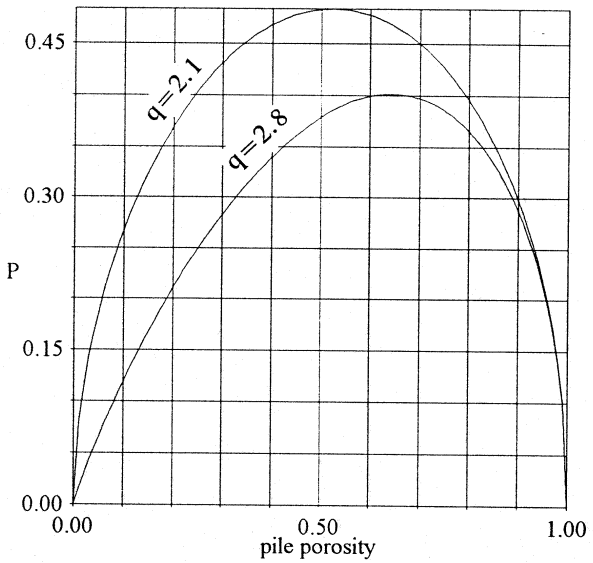


Fig. 4.1. Dependence of the porosity factor defined by eq. (4.14) on porosity values for high and low pH values (q=2.8 and 2.1 respectively).

Fig.4.1 shows the plots of P(ε) for values of q characteristic for low and high pH values. Additional strongly nonlinear effects appear as the result of discontinuities and cross-over effects discussed in the next section.

### 4.3 Bifurcations and Thermodynamic Catastrophes in Acid Generation Rates

Numerical values of the integral $I[U_m; U_b]$ show that the value of $\delta$ should be less than a certain critical value $\delta^*$ for which a transition to accelerated rates of acid production is expected. The values of $\delta^*$ depend on the scaling exponent, q, and are different for low and high pH values. The values of $U_b$ and $U_m$ in the integral define the temperature at the pile surface and the maximum temperature in the pile respectively (see eq. (4.8)). Figs. 4.2 and 4.3 present plots of the maximum value of U as the function of the scaling parameter $\delta$ for q=2.1 and two different values of $U_b$: $U_b$=0.0792 and $U_b$=0.13636 used later in Chapter V when various alternative scenarios are discussed. For $\delta=\delta^*=2.75$ in Fig. 4.2 we observe a discontinuity in $U_m$. Because the maximum temperature in the pile is proportional to $U_m$, we call this discontinuity a *thermodynamic catastrophe*. The thermodynamic catastrophe is responsible for accelerated rates of acid generation.

For given values of a and S the values of pile porosity and pile size should be controlled in such a way that the value of $\delta^*$ is not exceeded. The values of generation rates at $\delta>\delta^*$ can exceed by several times the acid generation rates at $\delta<\delta^*$ The critical values, $\delta^*$(pH) can be determined from numerical results obtained for the integral $I[U_m; U_b]$ which is a multivalued function of $U_m$ and $U_b$.

The curve $U_m(\delta)$ in Fig. 4.3 is continuous but also shows a dramatic increase in the vicinity of $\delta^*=2.35$. The critical value of the scaling parameter is defined in this case as the value of $\delta$ at which the maximum slope of the curve $U_m(\delta)$ occurs. The values of $\delta^*$ depend strongly on the temperature at the pile boundary. The greater the ambient temperature, the smaller the value of $\delta$ that should be maintained in order to avoid the thermodynamic catastrophe.

Chapter 5 demonstrates the practical use of the scaling parameter $\delta$ as the practical indicator of acid rock drainage. The qualitative features of the integral $I[U_m; U_b]$ for other values of the thermokinetic exponent q are the same as for the particular value of q=2.1 used in our examples. Thus the occurrence of thermodynamic catastrophes is a general feature of waste rock piles.

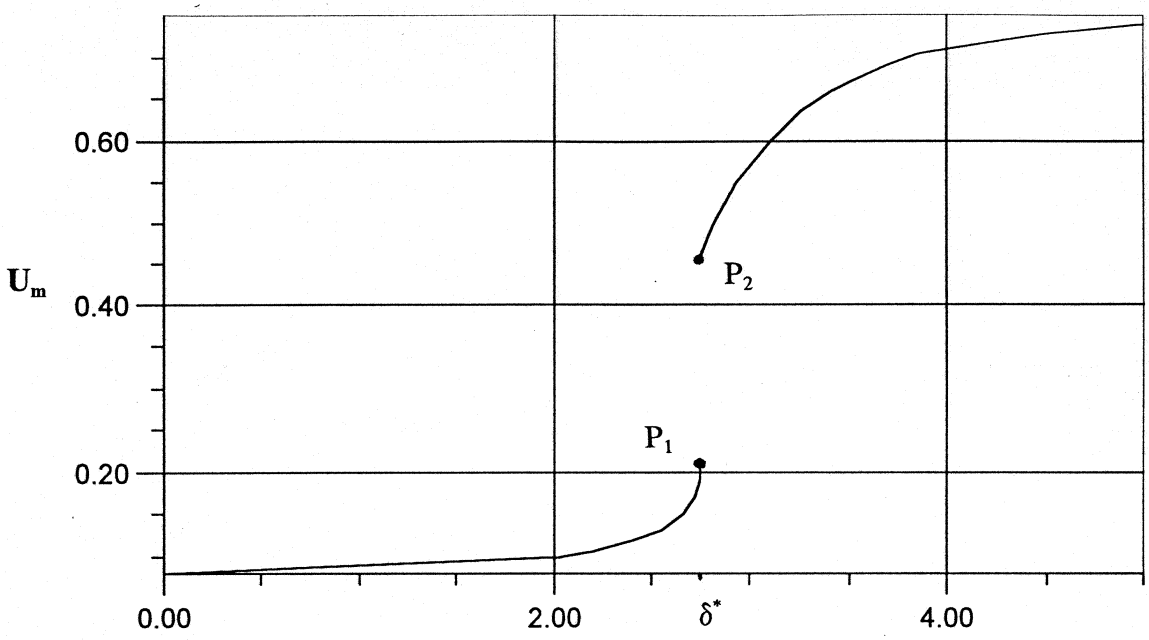


Fig. 4.2 Dependence of the maximum value of U (defined by eqs. (4.8)-(4.10)) on the values of the parameter δ; $U_b$=0.0792. At $\delta=\delta^*=2.75$ a discontinuity in the maximum temperature and acid generation rates occurs. (Note: The top branch extends beyond the point $P_2$ - this feature is not visualised here and is responsible for the thermodynamic hysteresis not discussed in this report)

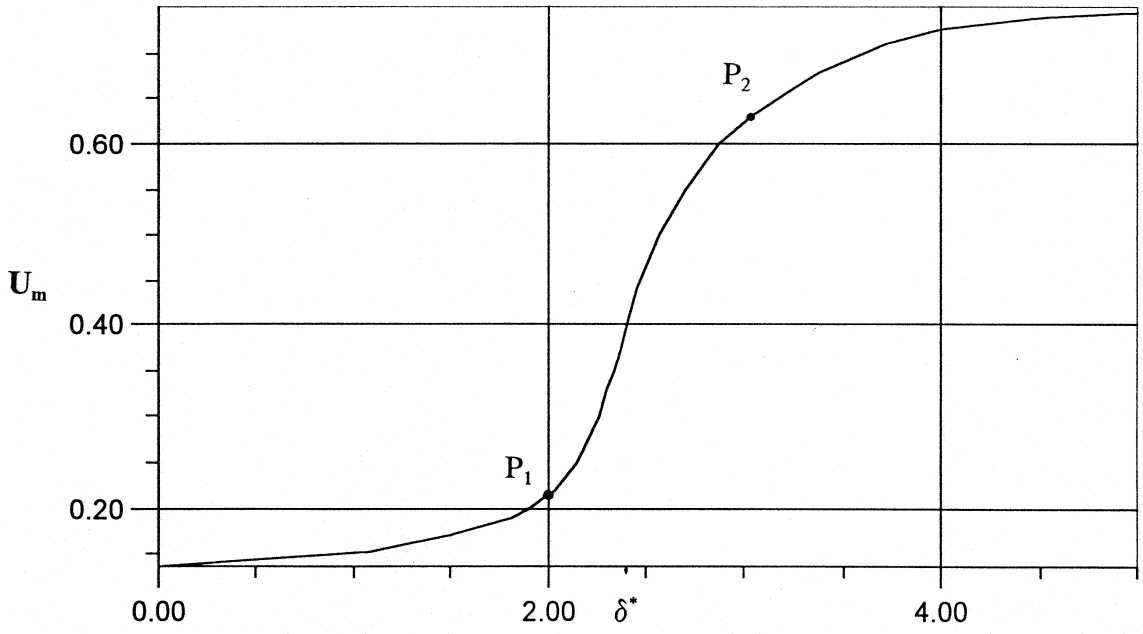


Fig. 4.3 Dependence of the maximum value of U (defined by eqs. (4.8)-(4.10)) on the values of the parameter δ; $U_b$=0.13636. In the vicinity of $\delta=\delta^*=2.35$ a dramatic increase in the maximum temperature and acid generation rates occurs.

## 5.0 PRACTICAL IMPLICATIONS OF PHYSICO-CHEMICAL SCALING RELATIONS

Scaling formulae derived in the Chapter 4 provide information about the relative importance of the chemical and physical factors responsible for ARD. The scaling relations can be used as a preliminary estimate of the expected ARD. In this section we demonstrate the use of the dimensionless parameter $\delta$ for different sets of entry data. We could not find in the literature *complete* entry data which would characterize any particular existing waste rock pile. Therefore we will use entry values coming from different sources, including values measured during small- and meso-scale laboratory experiments and field tests. The purpose of this chapter is to demonstrate the potential practical value of the scaling relations for different hypothetical scenarios. The more detailed analysis of expected acid concentrations in the effluent and a full validation of the model is left to a future study in which more realistic boundary conditions and the water transport will be included.

Most field data have been collected for waste rock piles in which convective oxygen transport played a significant role. It is known, however, that the convective air flow should be minimized and this can be done by using covers and placing waste rock piles on impermeable linings. Thus the results of this Chapter apply to properly designed piles with low porosity value and piles covered by low permeability covers. To our knowledge, this is the first study which uses the realistic chemical kinetics as a part of the physico-chemical model.

### 5.1 Alternative Scenarios of Acid Rock Drainage

In this Section, four different sets of entry data are used for our simple reaction-diffusion model. The two examples illustrate the possible range of variability of the dimensionless parameter $\delta$ and possible quantitative change in the type of nonlinear behaviour for different values of pile porosity. For different sets of entry data we find the conditions for the chemical kinetic coefficient $\alpha$ and pile size L necessary for the waste rock pile to remain in the low temperature regime. Scenarios 1 and 2 use small and intermediate porosity values. Scenarios 4 and 5 assume presence of impermeable covers resulting in a smaller than atmospheric concentration of oxygen at the cover - waste rock interface.

**Scenario 1:** *Small value of pile porosity*

We use the following set of entry data:

TABLE 5.1

| | |
|---|---|
| $\varepsilon = 0.13$ | (pile porosity) |
| $\lambda(\varepsilon) = 0.22$ J/(s m $^{o}$C) | (thermal conductivity) |
| h = 0.41 MJ/mol | (heat of pyrite oxidation per mol of oxygen consumed) |
| $D = 2.0 \cdot 10^{-5}$ m$^2$/s | (oxygen diffusion constant) |
| $a = 1.41 \cdot 10^{-10}$ ($^{o}$C)$^{-2.1}$m$^{-2}$s$^{-1}$ | (kinetic coefficient of the oxidation reaction) |
| S = 0.5 m$^2$ | (effective surface area of pyrite exposed to oxidation |

| | |
|---|---|
| | in $1m^3$ of pile volume) |
| q = 2.1 | (thermokinetic scaling exponent) |
| $T_b$= $10^oC$ | (temperature at the pile surface) |
| $Y_b$= 9.38 $mol/m^3$ | (oxygen concentration at the boundary) |

At first we calculate the maximum temperature $T^*_m$. $T^*_m$ is the upper bound on the maximum temperature in a pile. $T^*_m$ can be reached only in infinitely large piles. For the value of $T^*_m$ we obtain:

$$T^*_m = k\,Y_b + T_b = \frac{Deh\,Y_b}{l} + T_b = 55.5^o\,C \qquad (5.1)$$

Note that when ε goes to zero, there is no access of oxygen and $T^*_m$ equals the temperature at the surface, $T_b$. For large values of ε, in the absence of impermeable covers, the formula (4.7) cannot be used because the convective effects can no longer be neglected. For the values ofε between 0 and 0.25 the formula (4.7) gives a reasonable estimate.

For the adopted values of entry data the lower limit of the integral in formula (4.10) is given by:

$$U_b = \frac{U^*_m}{T^*_m} T_b = \frac{(q+1)T_b}{(q+2)(\frac{eDh\,Y_b}{l} + T_b)} = 0.13636 \qquad (5.2)$$

By using the formula $T=UT_m*(q+2)/(q+1)$ (see eq. (4.4); q=2.1) we obtain the dependence of the maximum temperature in the pile as the function of the dimensionless physicochemical universal scaling parameter δ. The plot presented in Fig. 5.1 is obtained from the universal plot in Fig.4.3 by rescaling the vertical axis by the factor:

$$g = \frac{T^*_m}{U^*_m} = \frac{q+2}{q+1} T^*_m \qquad (5.3)$$

Because γ defines the temperature scale, we call γ the *thermophysical coefficient.* Note that the thermophysical coefficient does not depend on the effective active surface area. The effective active surface area, S, appears in the formula for the scaling coefficient δ which defines the horizontal scale:

$$d = L\sqrt{\frac{2a(1e)}{(q+2)De}}\,[\frac{q+2}{q+1}(\frac{Deh\,Y_b}{l} + T_b)]^{q/2} \qquad (5.4)$$

where α=aS. The effective active surface area S seems to be the most difficult coefficient for estimation from the first principles.

In Fig. 5.1 two scales on the horizontal axis are used. For a given value of $\kappa=h\varepsilon D/\lambda$ and $T_b$, the plot 5.1 is valid for any combination of parameter values entering the formula (5.2) and for which $U_b$ remains unchanged. We have chosen the pile size, L, as a variable parameter. For fixed values of other parameters Fig. 5.1 illustrates the dependence of the maximum temperature in the pile as the function of the pile height, 2L. The length scale in Fig. 5.1 is defined by the formula ($\alpha=aS$; see also eqs. (4.9), (4.10) and (4.12)):

$$L = \frac{d}{\sqrt{\frac{2a(1e)}{(q+2)De}\left[\frac{q+2}{q+1}\left(\frac{DehY_b}{l}+T_b\right)\right]^{q/2}}} \qquad (5.5)$$

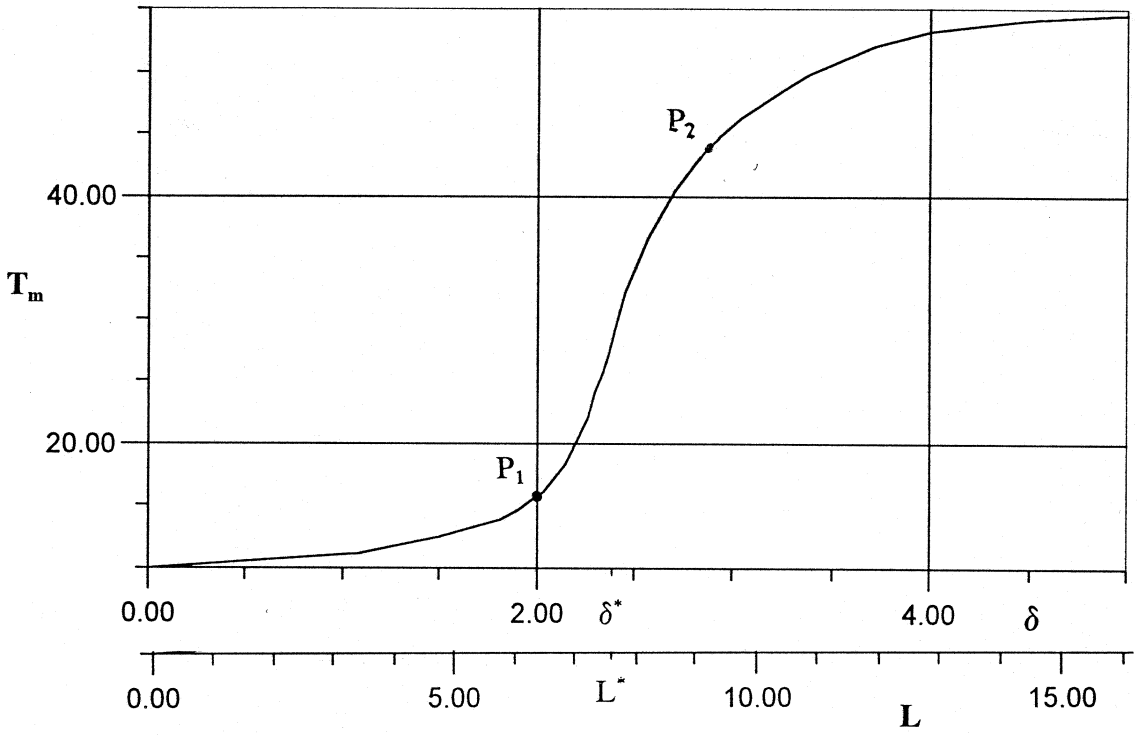


Fig. 5.1 Dependence of the maximum temperature (in °C) in the waste rock pile as the function of $\delta$ (upper horizontal scale) and pile size L (lower horizontal scale; L in meters). (The pile height is 2L)

In the analogous way, plots for any other values of the active surface area S can be obtained from a single plot 5.1. This property illustrates the universal character of the parameter $\delta$ given by formula (5.4). One can calculate the value of the scaling parameter $\delta$ based on the experimental data. The waste rock pile should be designed so that:

$$\delta < \delta^* \qquad (5.6)$$

In our example (see Table 5.1), for $\varepsilon$=0.13 and S=0.5 $m^2$ the pile height should be less than $2L^*$=15.2 m. When the condition (5.6) is satisfied, the maximum temperature in the pile is less than 30$^o$C. Analogous estimates can be made also in the presence of bacteria. In the presence of bacteria pyrite oxidation rates are much higher and the critical value of pile size, $L^*$ will be smaller. (One must remember, however, that the bacterial oxidation rates decrease with temperature at temperatures greater than 40$^o$C. For this reason qualitative behaviour of waste rock piles in the presence of bacteria is expected to be different than for abiotic oxidation. A separate scaling analysis is required when appropriate field studies will provide information about distribution of bacteria concentrations inside waste rock piles.)

The temperature profiles, T(x), for two different points $P_1$ and $P_2$ in Fig. 5.1, corresponding to two different values of $\delta$, are presented in Fig.5.2. The value $\delta_1$=2.0 is smaller than the cross-over value $\delta^*$=2.35 at which a thermodynamic catastrophe occurs. The value $\delta_2$=3.0 is greater than $\delta^*$. The value of $\delta^*$ is defined by the maximum slope of the curve in Fig. 5.1. (In our next example the value of $\delta^*$ is defined by the value of $\delta$ at which the discontinuity occurs (see discussion in Section 4.3).

Figs. 5.2 and 5.3 present plots of temperature as the function of the distance, x from the pile surface. Two particular values $L_1$=6.0 m and $L_2$=9.0 meters, which correspond to $\delta_1$=2.0 and $\delta_2$=3.0 are used. This example illustrates the cross-over effect. While $L_2$ is about 50% greater than $L_1$ , one observes a dramatic effect of size increase on the maximum temperature which changes from 15$^o$C to 45$^o$C. The pyrite oxidation rate at 45$^o$C is about 10 times faster than at 15$^o$C. Our analytical results are also supported by the numerical results obtained for the two trapezoidal piles with $L_1$=6.0 m and $L_2$=9.0 m and the base length equal to 100 meters. The temperature and oxygen profiles are presented in Appendix B. (The scaling analysis is also a good test for the numerical algorithm which we plan to use for more complex scenarios of ARD).

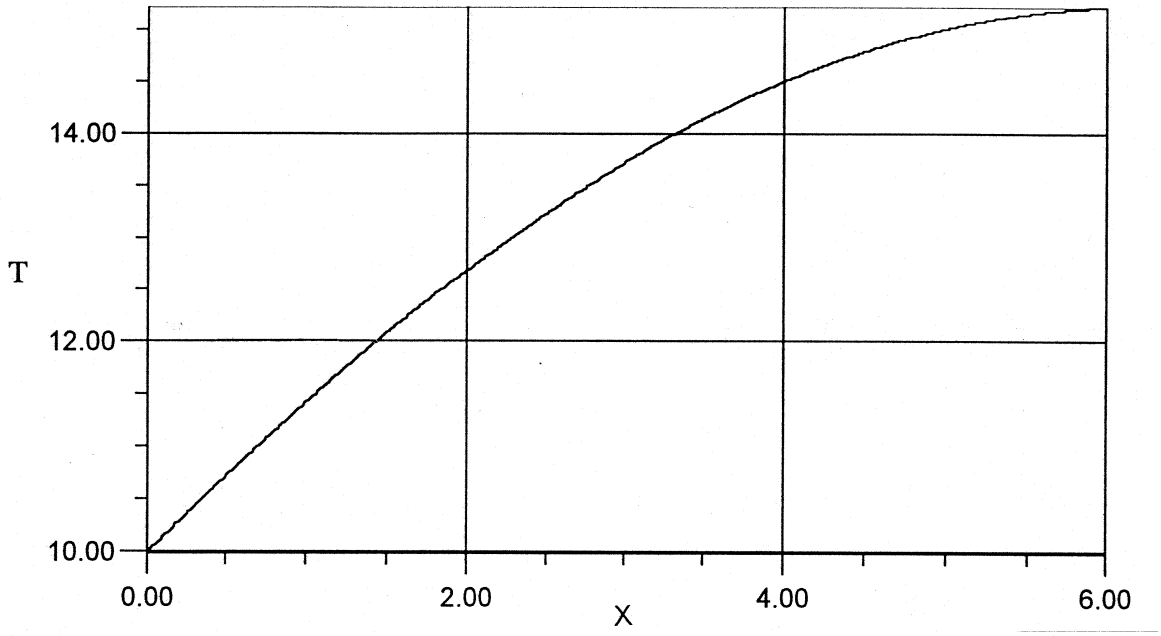


Fig. 5.2 Temperature profile T(x) as the function of the distance x from the pile surface for the point $P_1$ in Fig. 5.1. Pile height 2L=12 m. Parameter values are given in Table 5.1.

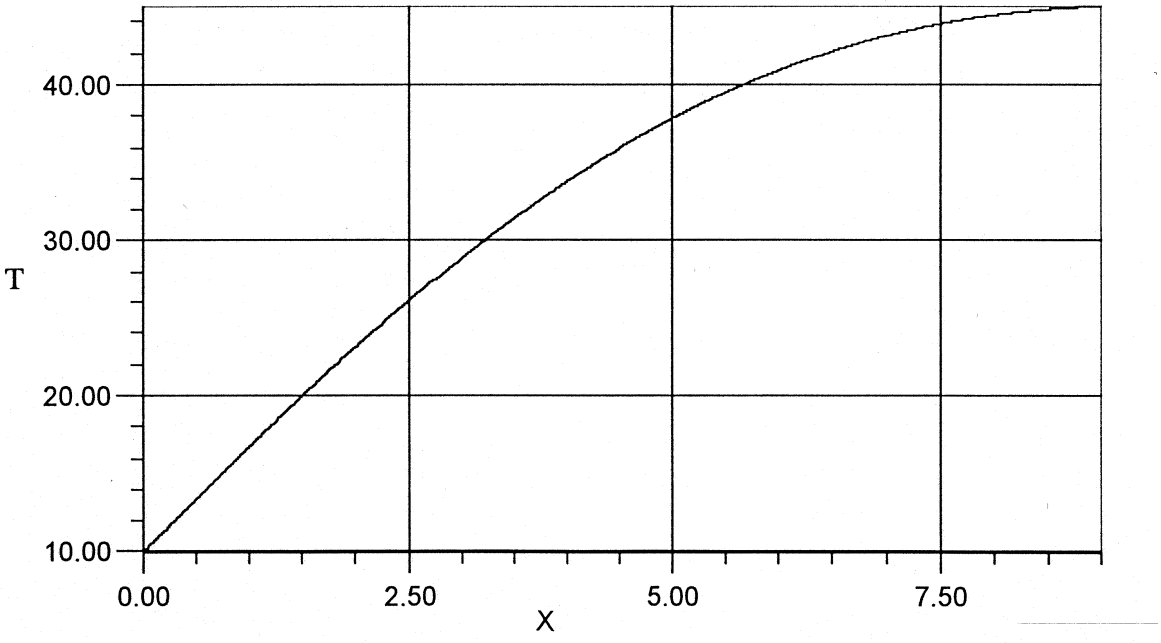


Fig. 5.3 Temperature profile T(x) as the function of the distance x from the pile surface for the point $P_1$ in Fig. 5.1. Pile height 2L=12 m. Parameter values are given in Table 5.1.

**Scenario 2:** *Moderate value of pile porosity*

In the second example, there is a greater value for pile porosity with a resulting smaller value of thermal conductivity. The following set of entry data is used:

TABLE 5.2

| | |
|---|---|
| $\varepsilon = 0.20$ | (pile porosity) |
| $\lambda(\varepsilon) = 0.18$ J/(s m $^{o}$C) | (thermal conductivity) |
| $h = 0.41$ MJ/mol | (heat of pyrite oxidation per mol of oxygen consumed) |
| $D = 2.0 \cdot 10^{-5}$ m$^2$/s | (oxygen diffusion constant) |
| $a = 1.41 \cdot 10^{-10}$ ($^{o}$C)$^{-2.1}$m$^{-2}$s$^{-1}$ | (kinetic coefficient of the oxidation reaction) |
| $S = 0.5$ m$^2$ | (effective surface area of pyrite exposed to oxidation in 1m$^3$ of pile volume) |
| $q = 2.1$ | (thermokinetic scaling exponent) |
| $T_b = 10^{o}$C | (temperature at the pile surface) |
| $Y_b = 9.38$ mol/m$^3$ | (oxygen concentration at the boundary) |

The same steps are followed as in the previous example. At first the temperature $T^*_m$ is calculated, which is the upper bound on the maximum temperature in a pile. For the value of $T^*_m$ we obtain:

$$T^*_m = k\,Y_b + T_b = \frac{Deh\,Y_b}{l} + T_b = 95.5^{o}C \qquad (5.7)$$

Once again we stress that $T^*_m$ cannot be reached in finite-size piles. To our knowledge, the maximum reported temperature measured during field tests is 75°C.

As a result of greater pile porosity and a smaller value of thermal conductivity, the present value of $T^*_m$ is greater than in Scenario 1. (The value of $T_b$=10$^{o}$C is the same as in Scenario 1.) The dependence of thermal conductivity on pile porosity is discussed by Schmal [Sch].

For the adopted values of entry data the lower limit of the integral in formula (4.10) is given by:

$$U_b = \frac{U^*_m}{T^*_m} T_b = \frac{(q+1)T_b}{(q+2)\left(\frac{eDh\,Y_b}{l} + T_b\right)} = 0.0792 \qquad (5.8)$$

In the next step we calculate the temperature profiles for two different points $P_1$ and $P_2$ in Fig. 5.4. $P_1$ and $P_2$ belong to two different thermodynamic branches at the critical value of $\delta=\delta^*=2.75$ at which the *thermodynamic catastrophe* occurs. (In Fig. 5.1 the value of $\delta^*$ is defined by the maximum slope of the curve $T(\delta)$). In the present example the value of the pile porosity is responsible for a smaller value of $U_b$ and this leads to the discontinuity at $\delta=2.75$.

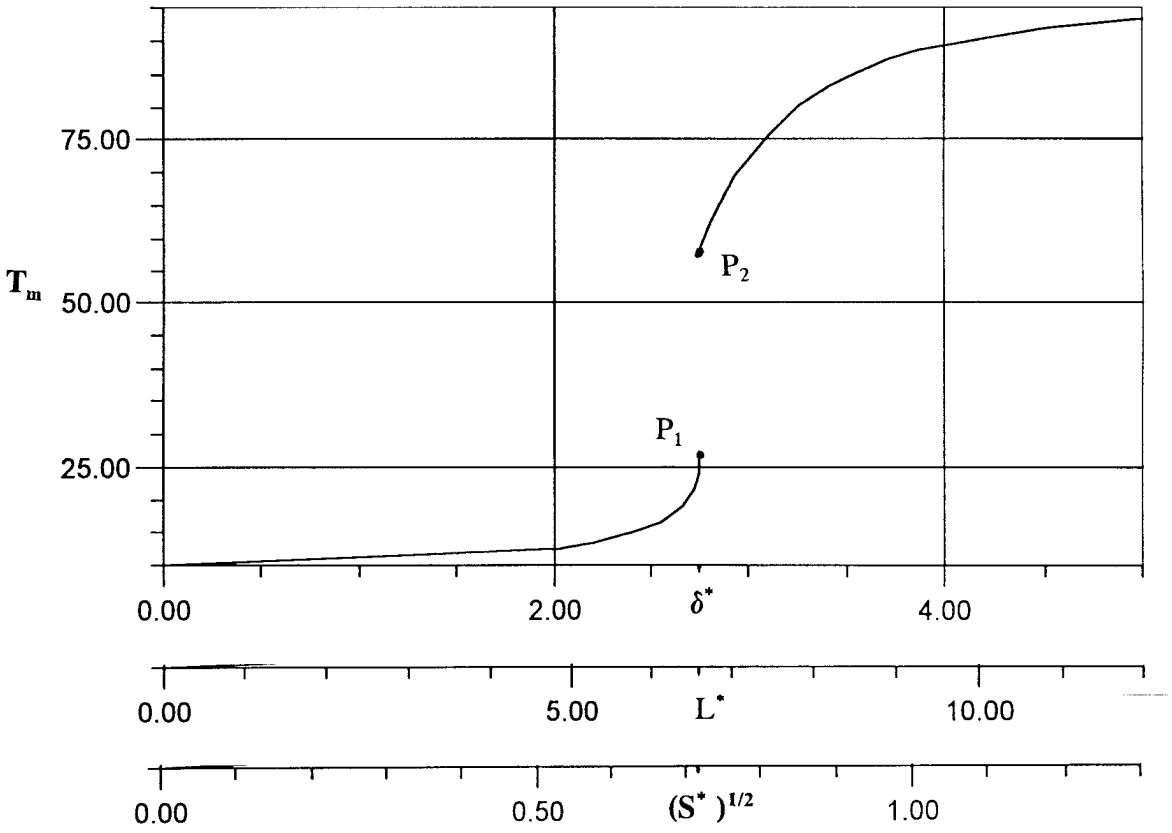


Fig. 5.4 Dependence of the maximum temperature in the waste rock pile as the function of: (a) scaling parameter $\delta$ ; (b) pile size L for S=0.5 $m^2$ (middle scale); (c) active surface area when L=6.5 m (lower scale).

In order to minimize the overall rate of acid generation the waste rock pile should be designed so that:

$$\delta < \delta^* = 2.75 \qquad (5.9)$$

As in the previous example, the plot presented in Fig. 5.4 is obtained from the universal plot in Fig. 4.2 by rescaling the vertical axis by the *thermophysical coefficient:*

$$g = \frac{T_m^*}{U_m^*} = \frac{q+2}{q+1} T_m^*$$

which does not depend on the effective active surface area, S. (S appears in the formula for $\delta$).

In the present example, for $\varepsilon$=0.20 and the same value of S as in Scenario 1, the pile height should be less than $2L^*$=13 m. This illustrates the general tendency that the cross-over value of L decreases with the increase of pile porosity. ($2L^*$ is equal to 15.2 m for $\varepsilon$=0.13 in Scenario 1).

In Fig. 5.4 three scales on the horizontal axis are used. For a given value of κ and $T_b$ the plot 5.4 is valid for any combination of parameter values entering the formula (5.8) and preserving the value of $U_b$=0.0792. When the horizontal scale in the middle is used, Fig. 5.4 represents the plot of the maximum temperature $T_m$ as a function of the pile size, L, when other parameters have fixed values given in Table 5.2. In addition to our previous example, we have also chosen the active surface area, S as a variable parameter. For the lowest horizontal scale, the pile size parameter has the fixed value 6.5 m. For fixed values of other parameters Fig. 5.4 with the lowest horizontal scale illustrates the dependence of the maximum temperature in the pile as the function of the effective active surface area, S. The lowest horizontal scale in Fig. 5.4 is defined by the formula:

$$\sqrt{S} = \frac{d}{L\sqrt{\frac{2a(1e)}{(q+2)De}}\left[\frac{q+2}{q+1}\left(\frac{DehY_b}{l}+T_b\right)\right]^{q/2}} \qquad (5.10)$$

For the pile of height 2L=13m, the thermal catastrophe occurs when the effective active surface area reaches the value $S^*$=0.5 $m^2$ . (From the scaling relation (5.10), $S^*$ is proportional to $1/L^2$ ; for the pile height of 15.2 m the critical value of $S^*$ becomes equal to 0.37)

Fig. 5.5 presents plots of temperature as the function of distance, x, from the pile surface for the critical value of L*=6.5 m when the thermodynamic catastrophe occurs (S=0.5 $m^2$). The maximum values of temperature reached for the two curves of T(x) are the same as the values of $T_m(P_1)$=26°C and $T_m(P_2)$=58°C in Fig. 5.4.

The oxygen concentration plots can be easily obtained by using eq. (4.3) (See Appendix B). The temperature and oxygen concentration profiles define the rate of acid generation discussed in the next section.

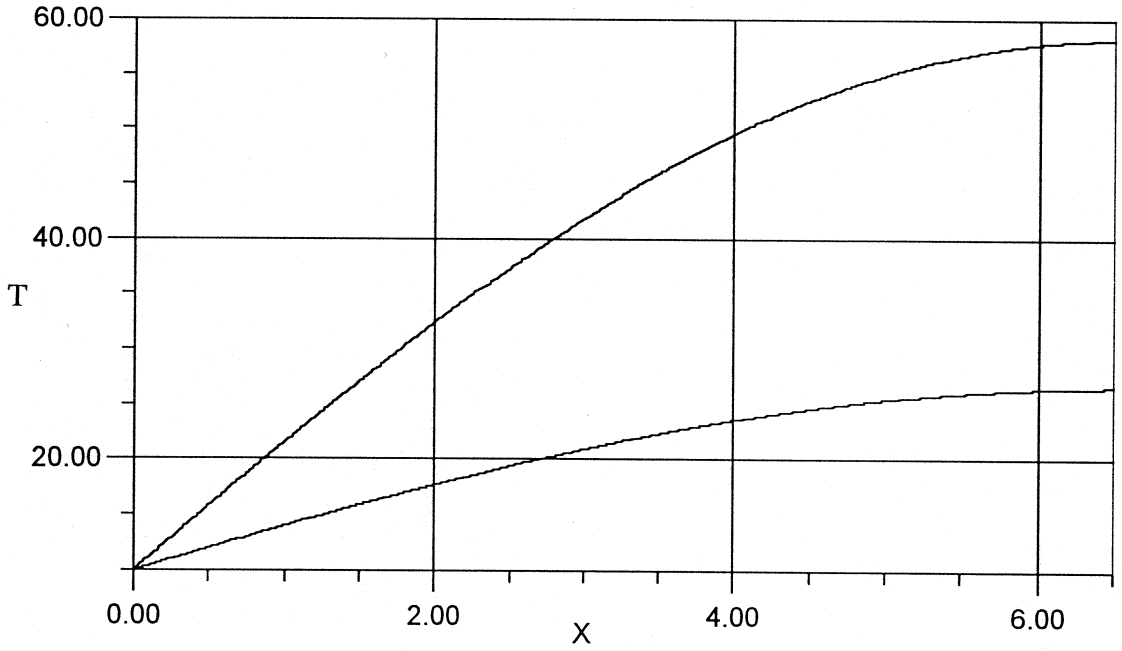


Fig. 5.5 Temperature profiles as the function of the distance x from the pile surface for the two points $P_1$ and $P_2$ on the lower and upper thermodynamic branches in Fig. 5.4. Parameter values are given in Table 5.2.

The same plots can be also used for other combinations of fixed and variable parameters. The same critical dependence of $T_m$ on $\delta$ occurs for arbitrary combinations of $\varepsilon$ and $T_b$ which produce the same value of $U_b$. For example, when in Scenario 2 the value of $T_b$=10°C is replaced by a new value of temperature at the pile surface, $T_b$=18.5°C, we obtain a plot of $U_m(\delta)$ with the same value of $\delta^*$ as in Fig.4.3. This happens because $\varepsilon$=0.20 and $T_b$=18.5°C produce the same value of $U_b$=0.13636 as $\varepsilon$=0.13 and $T_b$=10°C (see eq.(5.8)). In order to obtain the plots for $T_m(\delta)$, $T_m(L)$, $T_m(S)$ and T(x) one simply has to rescale the vertical axis of Fig. 4.3 by the thermophysical coefficient $\gamma$ and use eqs.(5.5), and (5.10) which define the horizontal scale.

In general, for any set of entry data it is sufficient to:

i) find the value of $U_b$ (eq. (5.2));
ii) calculate the universal function $U_m(\delta;U_b)$ to obtain a plot of $U_m(\delta)$ analogous to those in Figs. 4.2 and 4.3;
iii) use the definition of the thermophysical coefficient $\gamma$ (eq.(5.3)) to define the temperature scale (vertical axis); and
iv) use the definition of the scaling indicator $\delta$ to define the horizontal scale in terms of any variable (L, S,etc) entering the formula (5.4) for $\delta$.

This discussion illustrates the general value of the scaling relations. In the decision making process one can analyze different ways of managing the waste rock piles by using equivalent scenarios offered by the results of scaling analysis.

**Scenario 3:** *Large value of pile porosity and moderate-permeability cover*

In the third example, there is a large value for pile porosity with a resulting smaller value of thermal conductivity. In order to eliminate the detrimental effect of large pile porosity the entry data assume that a low permeability cover is applied in order to reduce oxygen access. This results in a smaller than atmospheric value of oxygen concentration at the interface between the cover and waste rock. We use a smaller value of $Y_b$ than in previous examples. The following set of entry data is used:

TABLE 5.3

| | |
|---|---|
| $\varepsilon = 0.28$ | (pile porosity) |
| $\lambda(\varepsilon) = 0.15$ J/(s m $^oC$) | (thermal conductivity) |
| $h = 0.41$ MJ/mol | (heat of pyrite oxidation per mol of oxygen consumed) |
| $D = 2.0 \cdot 10^{-5}$ m$^2$/s | (oxygen diffusion constant) |
| $a = 1.41 \cdot 10^{-10}$ ($^oC$)$^{-2.1}$m$^{-2}$s$^{-1}$ | (kinetic coefficient of the oxidation reaction) |
| $S = 0.5$ m$^2$ | (effective surface area of pyrite exposed to oxidation in 1m$^3$ of pile volume) |
| $q = 2.1$ | (thermokinetic scaling exponent) |
| $T_b = 15^oC$ | (temperature at the pile surface) |
| $Y_b = 1.88$ mol/m$^3$ | (oxygen concentration at the boundary) |

The present value of $Y_b$ corresponds to 5% oxygen concentration (21% is the normal atmospheric concentration.) The same steps are followed as in the previous examples. At first the temperature $T^*_m$ is calculated, which is the upper bound on the maximum temperature in a pile. For the value of $T^*_m$ we obtain:

$$T_m^* = k\,Y_b + T_b = \frac{Deh\,Y_b}{l} + T_b = 45.8^o\,C$$

Because of the impermeable cover, the present value of $T^*_m$ is similar to that in Scenario 1 despite the greater pile porosity and a smaller value of thermal conductivity (compare Table 5.1; the present value of $T_b$=15$^o$C is slightly higher as in Scenario 1.)

For the adopted values of entry data the lower limit of the integral in formula (4.10) is given by:

$$U_b = \frac{U_m^*}{T_m^*}T_b = \frac{(q+1)T_b}{(q+2)(\frac{eDh\,Y_b}{l} + T_b)} = 0.2478$$

Fig. 5.6 presents the dependence of the maximum temperature in the pile as the function of the scaling parameter $\delta$ and the pile size L. The critical values are $\delta^*$=2.0 and $L^*$=13 meters.

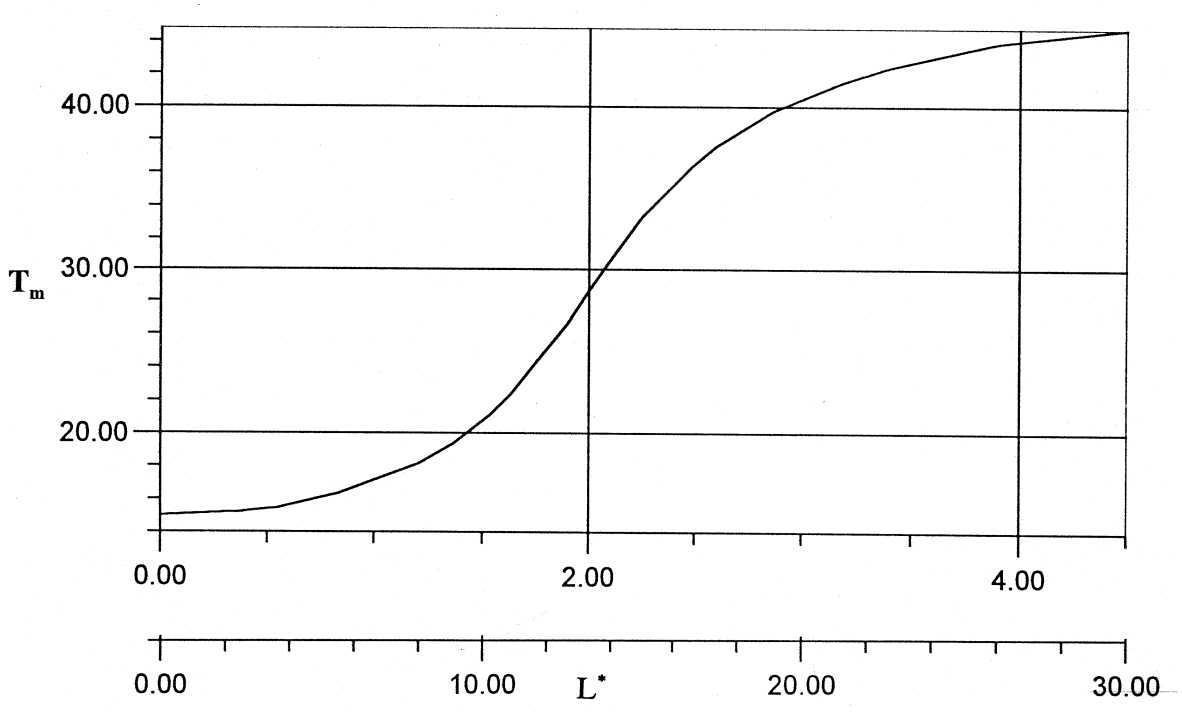


Fig. 5.6 Dependence of the maximum temperature in the waste rock pile as the function of: (a) scaling parameter $\delta$ ; (b) pile size L for S=0.5 $m^2$ (lower scale);

As in the previous examples, the temperature scale in the plot in Fig. 5.6 is determined by the *thermophysical coefficient:*

$$g = \frac{T_m^*}{U_m^*} = \frac{q+2}{q+1} T_m^*$$

which does not depend on the effective active surface area, S. (S appears in the formula for $\delta$).

In the present example, for $\varepsilon$=0.28, $Y_b$=1.88 mol/$m^3$ and the same value of S as in Scenarios 1 and 2, the cross-over value of L, $L^*$=13 m is obtained. $L^*$ is equal to 7.6 m for $\varepsilon$=0.13 in Scenario 1 (well compacted pile) and $L^*$ is equal to 6.5 m for $\varepsilon$=0.20 (moderately compacted pile) in Scenario 2 when no covers are used. The present example suggests that low-permeability covers should have a better effect than the pile compaction.

In general, the boundary value of oxygen concentration, $Y_b$, is a function of cover permeability and the total amount of oxygen consumed inside the pile per unit time. This aspect should be addressed in a more detailed numerical study.

**Scenario 4:** *Large value of pile porosity and poor cover*

In the fourth example, we again use a large value for the pile porosity with a resulting smaller value of thermal conductivity. A poor cover reduces the value of oxygen concentration at the interface between the cover and waste rock to a much lesser degree than in Scenario 3. We use the value $Y_b$ two times greater than in Scenario 3. The following set of entry data is used:

TABLE 5.4

| | |
|---|---|
| $\varepsilon = 0.28$ | (pile porosity) |
| $\lambda(\varepsilon) = 0.15$ J/(s m °C) | (thermal conductivity) |
| $h = 0.41$ MJ/mol | (heat of pyrite oxidation per mol of oxygen consumed) |
| $D = 2.0 \cdot 10^{-5}$ m$^2$/s | (oxygen diffusion constant) |
| $a = 1.41 \cdot 10^{-10}$ (°C)$^{-2.1}$m$^{-2}$s$^{-1}$ | (kinetic coefficient of the oxidation reaction) |
| $S = 0.5$ m$^2$ | (effective surface area of pyrite exposed to oxidation in 1m$^3$ of pile volume) |
| $q = 2.1$ | (thermokinetic scaling exponent) |
| $T_b = 15$°C | (temperature at the pile surface) |
| $Y_b = 4.69$ mol/m$^3$ | (oxygen concentration at the boundary) |

The present value of $Y_b$ corresponds to 10.5% oxygen concentration (21% is the normal atmospheric concentration). For the value of $T^*_m$ we obtain:

$$T^*_m = k\,Y_b + T_b = \frac{Deh\,Y_b}{l} + T_b = 84.2^o C$$

As a result of the higher cover permeability the present value of $T^*_m$ is much greater than in Scenario 3.

For the adopted values of entry data the lower limit of the integral in formula (4.10) is given by:

$$U_b = \frac{U^*_m}{T^*_m} T_b = \frac{(q+1)T_b}{(q+2)(\frac{eDh\,Y_b}{l} + T_b)} = 0.1307$$

Fig. 5.7 presents the dependence of the maximum temperature in the pile as the function of the scaling parameter $\delta$ and the pile size L.

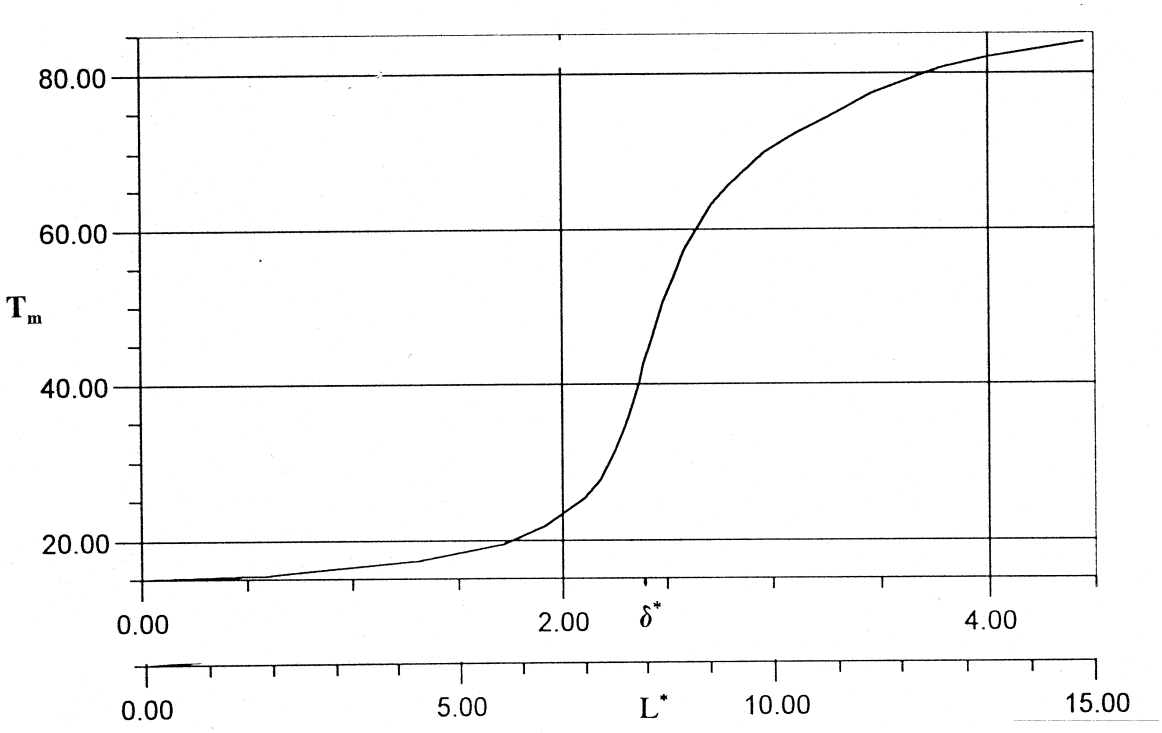


Fig. 5.7 Dependence of the maximum temperature in the waste rock pile as the function of: (a) scaling parameter $\delta$ ; (b) pile size L for S=0.5 $m^2$ (lower scale);

The critical values are $\delta^*$=2.4 and $L^*$=8.0 meters at which the maximum temperature $T_m$=40$^o$C. In Scenario 3 the same maximum temperature was reached in a much larger pile when L=19 m (see Fig. 5.6). This illustrates the general tendency that the allowed value of L increases with the decrease of cover permeability.

At large values of the maximum temperature, when $T_m$ is greater than 40$^o$C, the results for Scenario 4 are not expected to be very accurate because of the neglected convective air flow. In future work the results of scaling analysis should be extended to the situations when convective air flow and water infiltration rates are significant.

## 5.2 Acid Generation Rates

In the absence of bacteria, the acid generation rate is practically proportional to the oxygen consumption rate. We limit our attention to the qualitative features of the temperature dependence of acid generation rates.

Several existing linear models produce incorrect profiles of acid generation rate as the function of distance from pile surface. For the symmetric boundary conditions used in this study, the iron and sulphate production rates are given by the relations:

$$R_{Fe} = M_{Fe} e \frac{dY}{dt} = M_{Fe} (1e) a \, T^q (Y_b kT)^p \qquad (5.11)$$

and

$$R_{SO_4^2} = M_{SO_4^2} e \frac{dY}{dt} = M_{SO_4^2} (1e) a \, T^q (Y_b kT)^p \qquad (5.12)$$

The molar coefficients $M_{Fe}$=0.29 and $M_{SO42-}$=0.58 define the rates of iron and sulphate production in absence of bacteria, when quasi-equilibrium concentrations of ferric iron are small [SyT]. In general, the values of p and q have to be determined by laboratory tests discussed in Section 5.3.

Fig.5.8 presents the dependence of pyrite oxidation rate as the function of temperature for the same entry data as in Table 5.1 (Temperature profiles, T(x), are presented in Figs. 5.2 and 5.4; q=2.1 and p=1).

According to our mathematical analysis, the maximum acid generation rates occur at some distance from the pile surface, at the temperature $T_{Rm}(x_{Rm})$=37.5°C. For L=7.6 m in Scenario 1, the maximum pyrite oxidation rates occur close to the center of the pile at the distance $x_{Rm}$= 5 m from the pile surface. The maximum value of pyrite oxidation rate, 1.35 mol/(m$^3$s) corresponds to about 510 grams of pyrite per year per cubic meter.

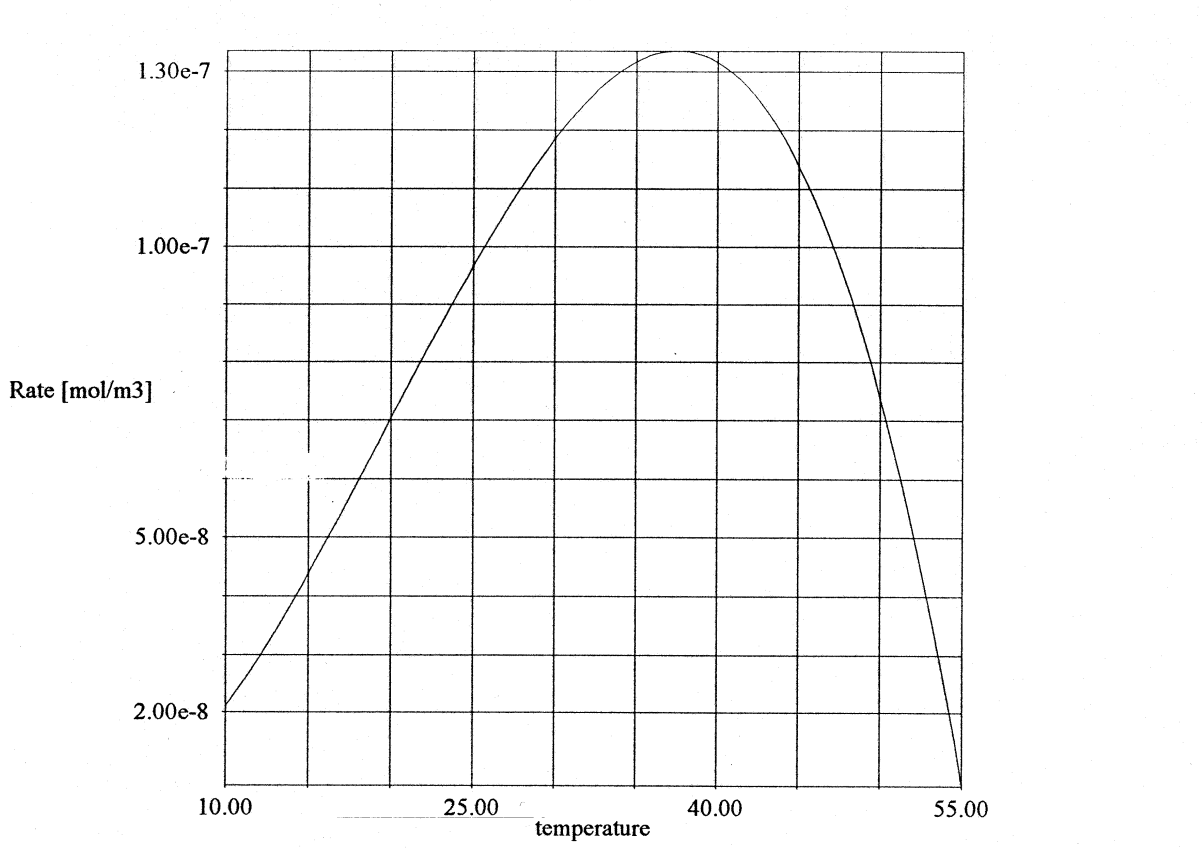

Fig. 5.8 Temperature dependence of pyrite oxidation rates expressed in units [mol/($m^3$s)]. The maximum pyrite oxidation rate occurs for an intermediate temperature value $T_{Rm}$=37.5°C. The value of $T_{Rm}$ is determined by the competitive effects of increasing temperature and decreasing oxygen concentration. The oxidation rate goes to zero when the temperature approaches the value $T_m^*$=54.5°C; $T_b$=10°C. The entry data listed in Table 5.1 are used.

The total acid generation rate increases 4 times as the result of the thermodynamic catastrophe at $\delta^*$=2.75 in Scenario 2. This is a dramatic effect indicating the importance of waste rock pile design. (The total acid generation rates can be obtained after integrating the profile R(x) over the pile volume).

For nonsymmetric boundary conditions, the oxygen concentration and temperature are related byeq. (4.3a). For the stronglynonsymmetric boundary conditions, the pyrite oxidation rates may show spatial oscillations. Such spatially oscillating patterns have been observed in Heath Steele [NoD]. (We have obtained approximate solutions expressed in terms of Bessel function for thenonsymmetric boundary problem - the discussion of this problem goes beyond the scope of the scaling analysis presented in this report).

## 5.3 Required Accuracy of Laboratory and Field Tests

Acid generation rates depend critically on the value of the physico-chemical scaling parameter $\delta$ given by eq. (5.4). The scaling parameter $\delta$ can be calculated for a wide range of physical conditions characterized by the temperature $T_b$ at the pile surface and pile porosity, $\varepsilon$. The chemical properties of waste rock can be characterized by the kinetic coefficient, *a*, and the effective active surface area, S. The value of S depends on several factors including the total content of pyrite, pyrrhotite and other sulphur compounds, the effective value of rock porosity, rock morphology, etc. In particular, one may measure rock porosity by means of the fractal dimension of pores. We feel, however, that the complexity of elementary factors responsible for the ARD potential is so high, that one should rely on the results of simple laboratory tests. Such tests should be performed for different values of temperature and different oxygen partial pressures in order to define the scaling curve $\alpha T^q$ and the exponent, p, for the oxidation process. Representative samples of waste rock should be used for such tests. For the needs of a predictive model it would be sufficient to perform oxidation tests under isothermic conditions at temperature intervals of 15°C in the temperature range between 5°C and 80°C and oxygen partial pressures varying between 0.21 atm and 0.01 atm at 0.05 atm intervals. Such isothermic tests should be performed at water saturation values characteristic for waste rock piles. In this way one can produce in a relatively inexpensive way the input data sufficient for a predictive model. This approach seems to be more practical than the approach based on a more direct measurement of the effective reactive surface area, S, and fractal dimensions of pores. One has to realize that microscopic factors such as the content of different morphological forms of pyrite can vary the value of S by a factor of two. The surface areas exhibited by pyrite of different morphologies vary from $6.5 \times 10^{-3}$ $m^2/g$ for euhedral morphology to $1.2 \times 10^{-2}$ $m^2/g$ for subhedral/framboidal morphologies [WhJ]. Variation of surface area as the function of pyrite particle size is another important microscopic factor.

The value of heat, h, generated during the pyrite oxidation process can be different for different values of acid neutralization potential. We could not find reliable data on the heat generated by calcite dissolution or the neutralization reactions, which would modify the value of h used in this report. We do not recommend, however, to measure these quantities separately. The cumulative heat generated during the weathering process is sufficient for the predictive reaction-transport model. The heat generated can be measured in the same isothermal experiment (proposed above) as the value of cooling necessary to preserve constant temperature of the oxidation process. In this way we can keep the same number of measurable coefficients as in our scaling model in which only the effective heat of pyrite oxidation is analyzed.

We also perform a simple error analysis for the scaling coefficient $\delta$. The relative contributions due to the variation of different measurable parameters indicate the required accuracy of experimental tests. The estimated relative variation $\delta_f$ is given by:

$$\frac{\Delta d}{d} = \left(\frac{e}{2} + \frac{q1}{2}\right)\frac{\Delta e}{e} + \frac{q}{2}\frac{\Delta l}{l} + \frac{q}{2}\frac{\Delta h}{h} + \frac{1}{2}\frac{\Delta a}{a} \qquad (5.13)$$

The above formula assumes that the exact value of D is known. Our rather lengthy analysis which we do not present here, shows that the error in q has a negligibly small effect on $\delta/\delta^*$ and for this reason there are no terms proportional to $\Delta q$ in eq.(5.13).

If we assume, somewhat arbitrarily, the relative accuracy $\Delta\delta/\delta$ should be better than 25%, then we obtain the following estimate for the accuracy of the parameters involved when q=2.1:

$$\Delta h/h = 10\ \%, \quad \Delta\varepsilon/\varepsilon = 10\ \%, \quad \Delta\lambda/\lambda = 10\ \%, \quad \Delta\alpha/\alpha = 15\ \% \qquad (5.14)$$

We have allowed a 10 % error for the directly measured simple quantities, and a 15% error for the effective coefficient $\alpha$ which has to be determined from a series of results and usually varies even in waste rock from the same source. A sample of waste rock with the particle size representative for the pile should be used to determine the parameter $\alpha$=aS. Usual acid/base accounting tests do not provide data necessary for a predictive model which should generate quantitative information about the effluent.

If the indicated accuracy of the experimental data is achieved, the waste rock pile should be designed so that the condition:

$$d < 0.75\, d^* \qquad (5.15)$$

is satisfied.

We hope that the last condition can be used as a practical and simple guideline for designing waste rock piles. Better estimates can be produced by a numerical model which should use nonsymmetric boundary conditions and include convective effects. When the waste rock pile is placed on the impermeable lining, the maximum allowed value of $\delta$ will increase provided the impermeable lining does not lower the heat transport rate. The present model has to be validated by using results of available laboratory and field tests before adopting the results of this study as practical guidelines.

## 5.3 Discussion of Results

The examples (Scenarios 1-4 in Section 5.1) illustrate the practical power of the scaling relations. Results for various combinations of physical and chemical parameters characterizing waste rock and pile design, can be obtained without repeating the numerical calculations for every new set of entry data.

Analogous estimates can be made also in the presence of bacteria. In the presence of bacteria pyrite oxidation rates are much higher and the critical value of pile size, $L^*$ will be lower. The activation energy of pyrite oxidation by ferric iron is greater than the activation energy of oxidation by oxygen. For this reason the model involving the bacterial oxidation will use a different value of the nonlinear thermokinetic exponent q and additional nonlinearity will be introduced by the temperature dependence of bacterial oxidation $S_y$[T], [Se].

While the sample calculations are performed for pyrite, the same model with only slight modifications can be used for other acid generating minerals. Useful scaling relations can also be derived in the presence of water transport and air convection.

Unlike the existing waste rock models, the kinetic equations used in this study do not contain adjustable parameters. All the parameters entering eqs. (4.1) and (4.2) can be measured in a series of independent experiments. At the same time we do not pretend that the equations (4.1), (4.2) and their steady state solutions provide a complete description of waste rock piles. The kinetic model used for our scaling analysis assumes that:

- the convective transport of oxygen is slow;
- the water flow is slow;
- the pile is large and seasonal temperature changes affect a small external portion of the pile;
- the waste material has a uniform pyrite concentration throughout the pile; and
- water vapour concentration is uniform inside the pile so that the diffusion coefficient D remains constant.

The first two assumptions should be adopted as a practical rule for waste rock management and therefore should be considered as realistic features of waste rock piles. (Different principles have to be adopted when the preemptive leaching is used - see comment on p.24). The first four assumptions are not satisfied in the case of most field-study reports available through MEND. In particular, piles 17, 18a and 18b in the Heath Steele study were small (only 4-5m high), had high porosity and were not placed on impermeable lining (thus allowing high flux of oxygen from the base). In such cases the oxidation rates are limited not by diffusive oxygen transport but by the convective transport of thermal energy and convective oxygen transport. This is an undesirable situation leading to temperatures above $40^oC$ despite a small pile size. In the case of Mine Doyon only the third assumption is satisfied and the estimated thermal energy stored in the pile is equivalent to about 2.5 years of the thermal activity of the waste material. This results in relatively small seasonal temperature variations at distances greater than 5 meters from the pile surface (see Fig. 4 on p. 33 of [LGI]). Because of the large thermal inertia the seasonal changes in Mine Doyon's dump remain small despite high convection rates.

We concentrate our attention on diffusive transport because it seems that the convective transport should be eliminated in properly managed waste rock piles. (A model which will properly describe convective effects should be analyzed, however, in order to understand ARD for a broad range of conditions). Even when convective transport is eliminated, the nonlinear effects which were disregarded in existing numerical models, are responsible for thermal catastrophes leading to an abrupt increase in the acid generation rates when the critical value $\delta^*$ of the physico-chemical scaling parameter is reached. For large values of the scaling indicator $\delta$, the pyrite oxidation rates with diffusive oxygen transport become as high as in the presence of convection. In order to understand this feature one has to realize that rates of oxygen supply while increasing due to convection, are accompanied by increased rates of energy transport to the surroundings. The scaling analysis can be easily performed also when convective mass and energy transport becomes dominant. One of the main differences is the proportionality of acid generation rates to $\alpha$ instead of $\alpha^{1/2}$ - this results in a more dramatic increase of the acid generation rates with respect to the pyrite content of waste rock.

A sample of numerical solutions obtained by the finite elements method is presented in Appendix B. The numerical results confirm the analytical results of the scaling analysis.

Our main purpose was to demonstrate that the chemical parameters measured in small-scale and meso-scale laboratory experiments can be combined with large-scale physical parameters (like pile size, for example) and that a physico-chemical model can produce a realistic description of the large-scale thermo-chemical behaviour of waste rock piles. Having demonstrated that the simple model derived from fundamental physical and chemical principles gives reasonable results, we feel confident that after a further refinement it is possible to construct a realistic and useful waste rock model.

## 6.0 CONCLUSIONS AND RECOMMENDATIONS

A physico-chemical model can produce a realistic description of a large-scale thermo-chemical behaviour of waste rock piles. Having demonstrated that the simple model derived from fundamental physical and chemical principles gives reasonable results, we feel confident that after a further refinement it is possible to construct a realistic and useful waste rock model.

Scaling analysis of a nonlinear reaction-transport model has been performed. The acid generation rates can be characterized by a physico-chemical scaling parameter $\delta$ which depends on pile porosity, pile size, ambient temperature, effective reactive pyrite surface area, heat of oxidation and thermal conductivity. The scaling parameter $\delta$ can be used as a practical indicator of ARD. The scaling parameter provides quantitative information about the relative importance of the factors responsible for acidic drainage. In particular, the effectiveness of impermeable covers increases with the pyrite concentration. Sample calculations of temperature profiles and acid generation rates have been performed for realistic parameter values in the absence of bacteria and without neutralization. Alternative scenarios with and without impermeable covers are discussed.

The scaling analysis indicates that geochemical and transport processes operate at the meso-scale in a way fundamentally different from the full-scale. When oxygen supply is controlled by the diffusion process, the waste rock piles can exhibit thermodynamic catastrophes. A thermodynamic catastrophe occurs when relatively small changes of parameters, such as pile size, pile porosity, ambient temperature or effective active surface area result in a dramatic increase of the acid generation rate. The scaling parameter $\delta$ provides quantitative information about waste rock storage conditions, such as pile porosity and pile size, which have to be satisfied in order to avoid a thermodynamic catastrophe leading to accelerated acid generation rates.

The scaling analysis indicates that in order to avoid a thermodynamic catastrophe leading to high acid generation rates, the waste rock piles should be designed so that the value of the physico-chemical scaling parameter $\delta$ is less than a critical value $\delta^*$. Illustrative examples of the practical applications of the critical scaling criterion are presented.

In the next step, air convection and water transport should be included in the model and quantitative results for the expected water quality should be obtained.

In an additional study one should analyze the problem of optimum pile shape as the function of the cover permeability and the total amount of waste rock to be stored.

All the quantities involved in the scaling analysis can be measured in independent simple laboratory experiments. The accuracy of simple experiments sufficient for a predictive waste rock model has been analyzed. Because realistic results are obtained with no additional adjustable parameters, we believe that after experimental validation and additional refinement (involving nonsymmetric boundary conditions, water transport and convection of air) the results of the scaling analysis can be used as simple practical guidelines for design of waste rock sites.

Quantitative information about the oxygen consumption by bacteria and the spatial distribution of bacteria concentration in waste rock piles is necessary for extending the present scaling analysis to the case of bacterial oxidation by *Thiobacillus ferrooxidans*. When such data become available, the quantitative results for bacterial oxidation reviewed in our previous study [SyT] can be used to modify the present scaling analysis.

One should rely on the results of simple laboratory tests. In addition to the usual acid/base accounting tests, thermokinetic tests should be performed for different values of temperature, pH and different oxygen partial pressures in order to define the scaling curves $Y^p$ and $\alpha T^q$ which are expected to be different for rocks with different neutralization potential. Representative samples of waste rock should be used for such tests. For the needs of a predictive model it would be sufficient to perform oxidation tests under isothermic conditions at temperature intervals of $15^oC$ in the temperature range between $5^oC$ and $80^oC$ and oxygen partial pressures varying between 0.21 atm and 0.01 atm at 0.05 atm intervals. The same experiments should also measure the cumulative heat of oxidation/neutralization reactions. Such isothermic tests should be performed separately for pH greater than four and pH less than four in the presence of bacteria, at water saturation values characteristic for waste rock piles. For small pH values bacteria concentration and oxygen consumption should be monitored for different values of oxygen partial pressure. In this way one can produce in a relatively inexpensive way the input data necessary for a predictive model which should help to optimize the storage of waste rock and to provide a reliable tool useful for environmental assessment. Usual acid/base accounting tests do not provide data necessary for a predictive model which should generate quantitative information about the effluent.

The value of heat, h, generated during the pyrite oxidation process can be different for different values of the acid neutralization potential. We could not find reliable data on the heat generated by calcite dissolution or the neutralization reactions, which would modify the value of h used in this report. We do not recommend, however, to measure these quantities separately. The cumulative heat generated during the weathering process is sufficient for the predictive reaction-transport model. The heat generated can be measured in the same isothermal experiment (proposed above) as the value of cooling necessary to preserve constant temperature of the oxidation process. In this way we can keep the same number of measurable coefficients as in our scaling model in which only the effective heat of pyrite oxidation is analyzed.

## APPENDIX A

### Numerical results for the chemical kinetics at different pH values

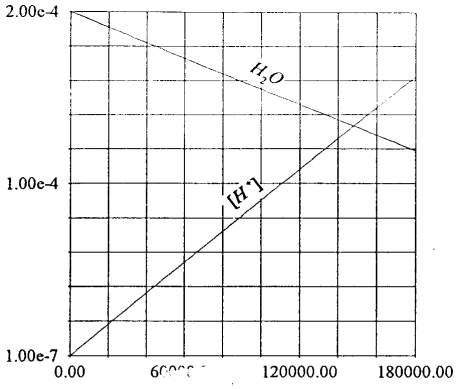


(11)

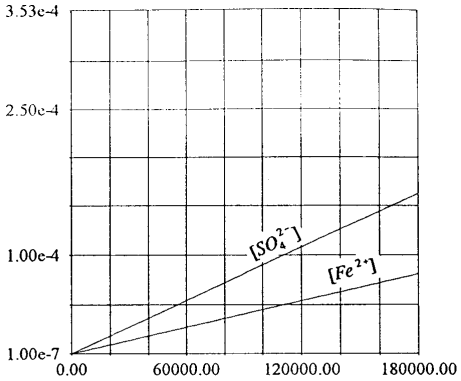


(12)

T=283K

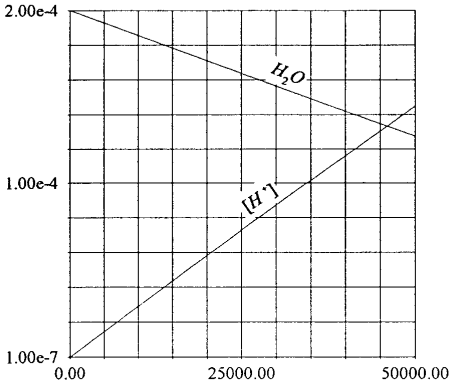


(21)

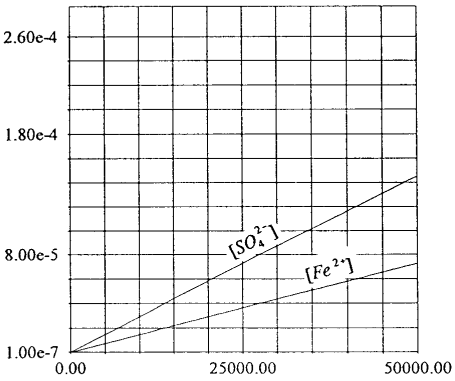


(22)

T=293K

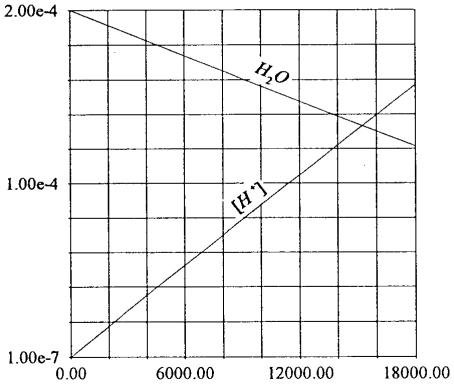


(31)

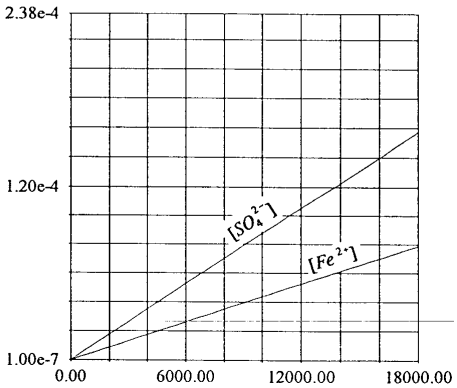


(32)

T=303K

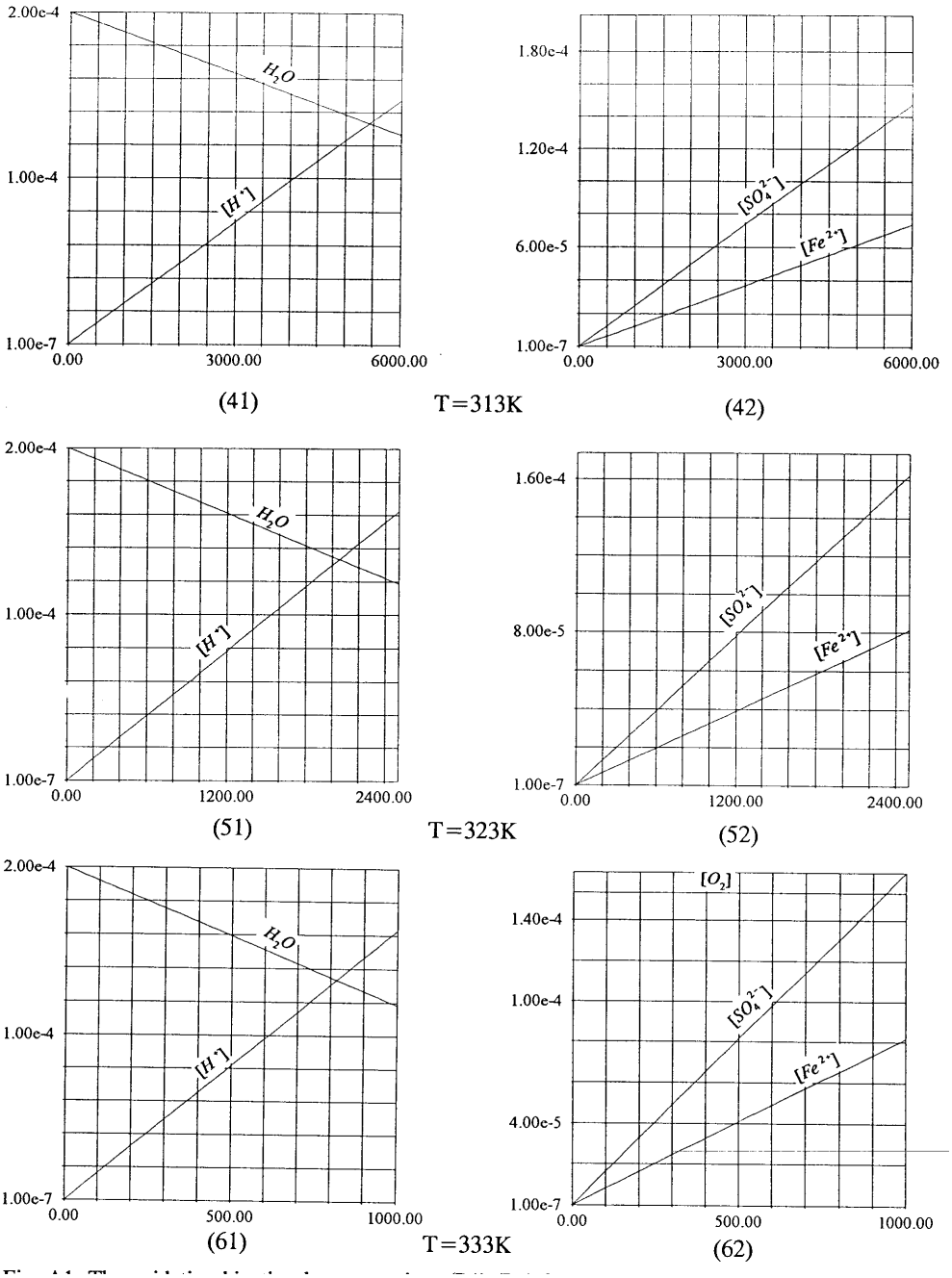


Fig. A1. The oxidation kinetics due to reactions (R1)-(R4) for different temperatures; S/V=10 $m^2$/l and the initial conditions: $[Fe^{2+}(t=0)]=0$, $[SO_4^{2-}(t=0]=0$, $[Fe(OH)_3(t=0)]=0$ and pH(t=0)=7. Constant in time concentration of dissolved oxygen, $[O_2]$ for $[O_2]_{gas}=21\%$. Horizontal axis: time in seconds, vertical axis: concentration in moles per litre. (180 000 sec = 5 hours).

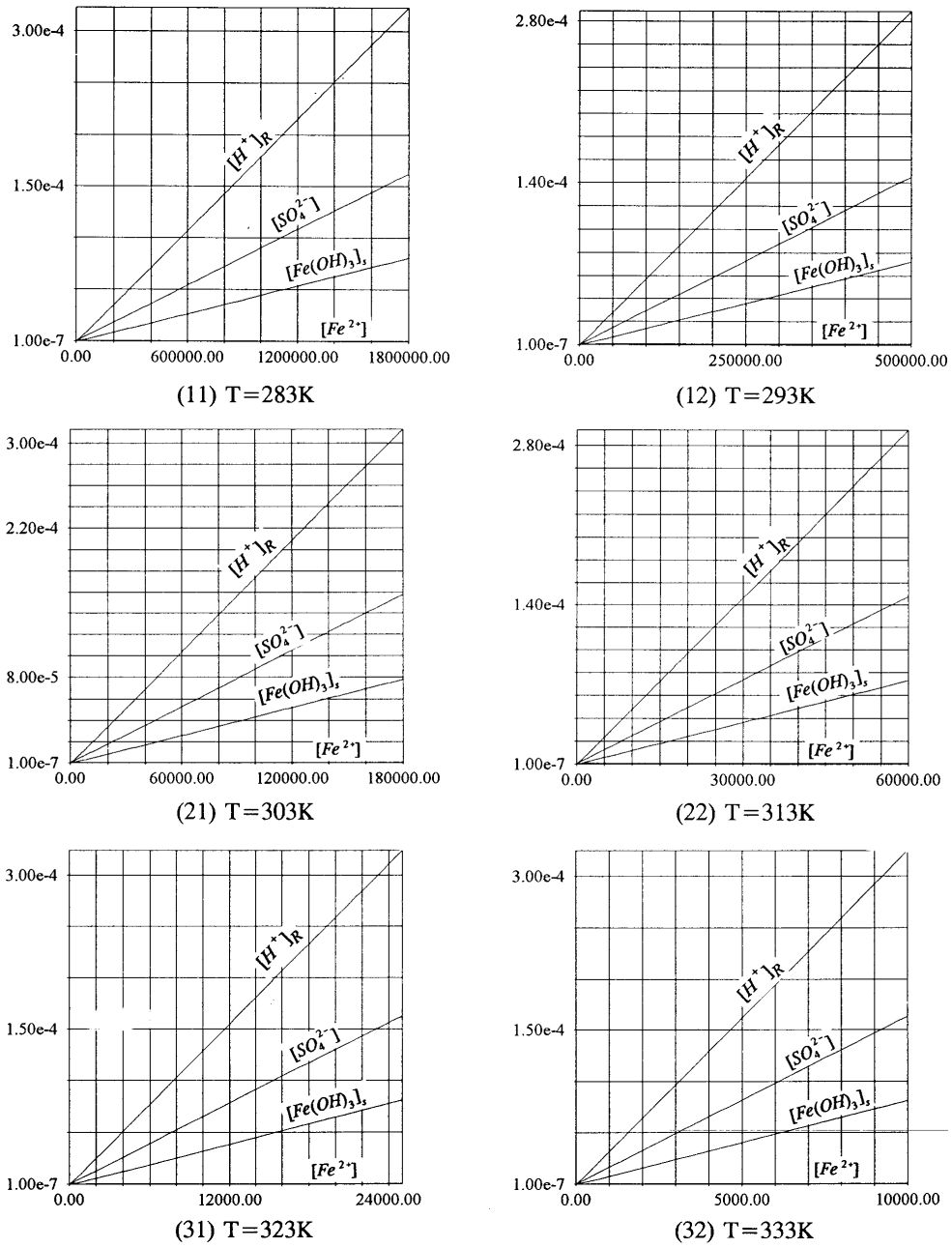


Fig. A2. The oxidation kinetics due to reactions (R1)-(R4) for different temperatures, S/V=1 $m^2/l$; the initial conditions: $[Fe^{2+}(t=0)]=0$, $[SO_4^{2-}(t=0]=0$, $[Fe(OH)_3(t=0)]=0$. Constant in time pH(t=0)=6.9 concentration of dissolved oxygen, $[O_2]$ for $[O_2]_{gas}=21\%$. Horizontal axis: time in seconds, verticalaxis:concentration in moles per litre. (1 800 000 sec = 3 weeks).

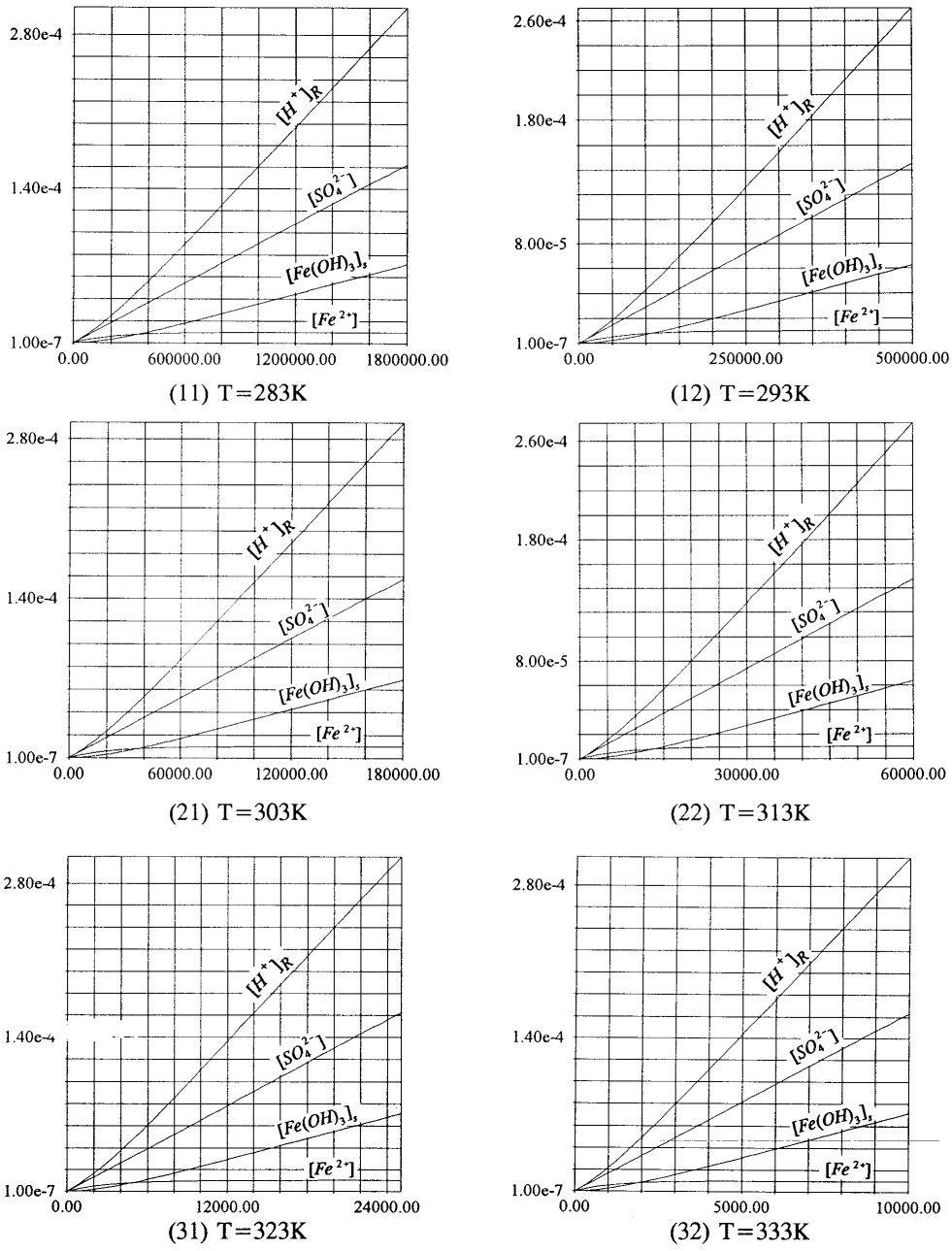


Fig. A3. The oxidation kinetics due to reactions (R1)-(R4) for different temperatures, S/V=1 $m^2/l$; the initial conditions: $[Fe^{2+}(t=0)]=0$, $[SO_4^{2-}(t=0]=0$, $[Fe(OH)_3(t=0)]=0$. Constant in time pH(t=0)=6.3 concentration of dissolved oxygen, $[O_2]$ for $[O_2]_{gas}=21\%$. Horizontal axis: time in seconds, verticalaxis:concentration in moles per litre. (1 800 000 sec = 3 weeks).

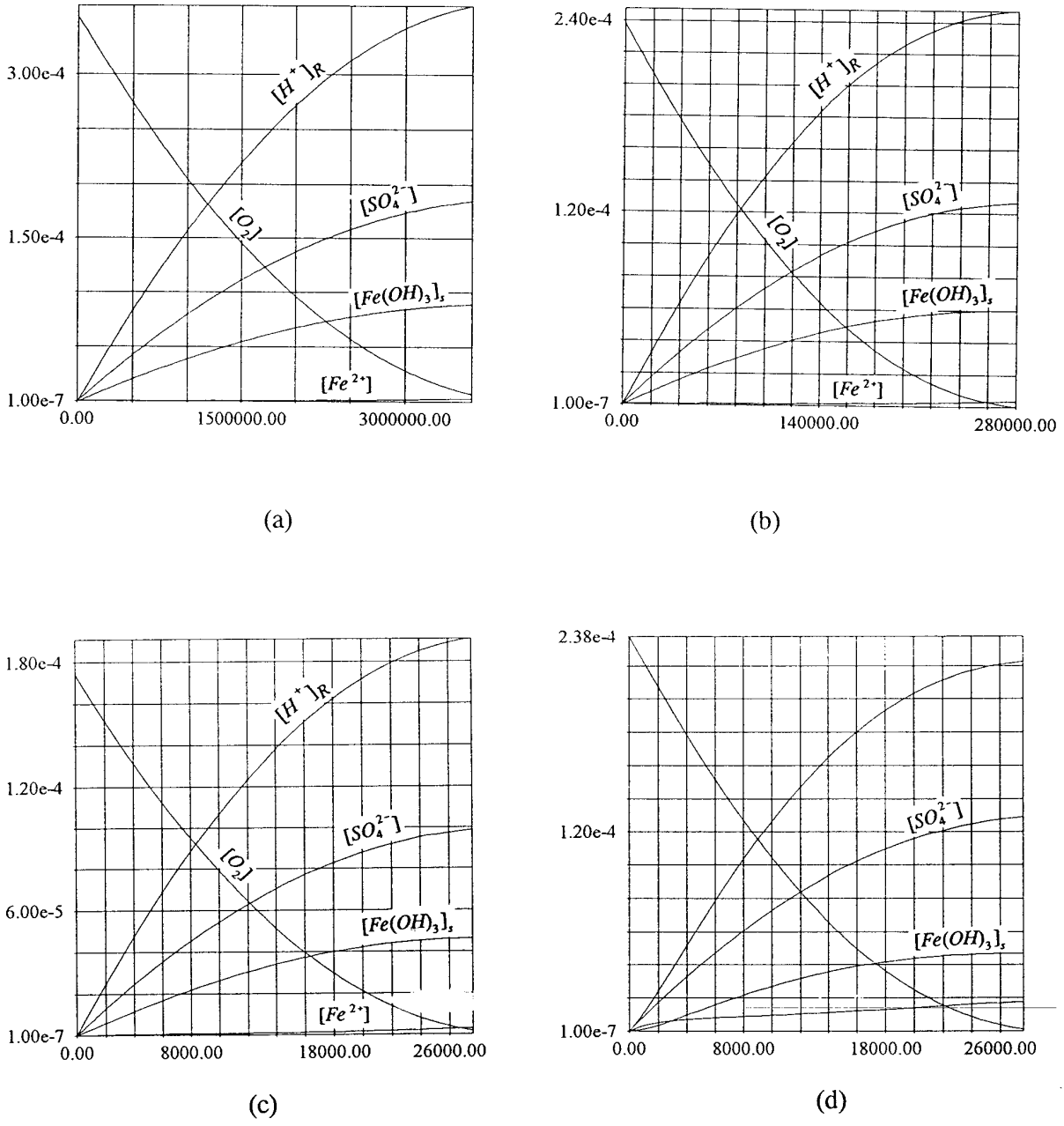


Fig. A4. The consumption of dissolved oxygen at pH=6.9 for different values of S/V and different temperatures. (a) S/V=1m$^2$/l, T=283 K; (b) S/V=1m$^2$/l, T=303 K; (c) S/V=1m$^2$/l, T=323 K; (d) S/V=10m$^2$/l, T=303 K. Horizontal axis: time in seconds; vertical axis: concentration in moles per litre (3 000000 s=35 days).

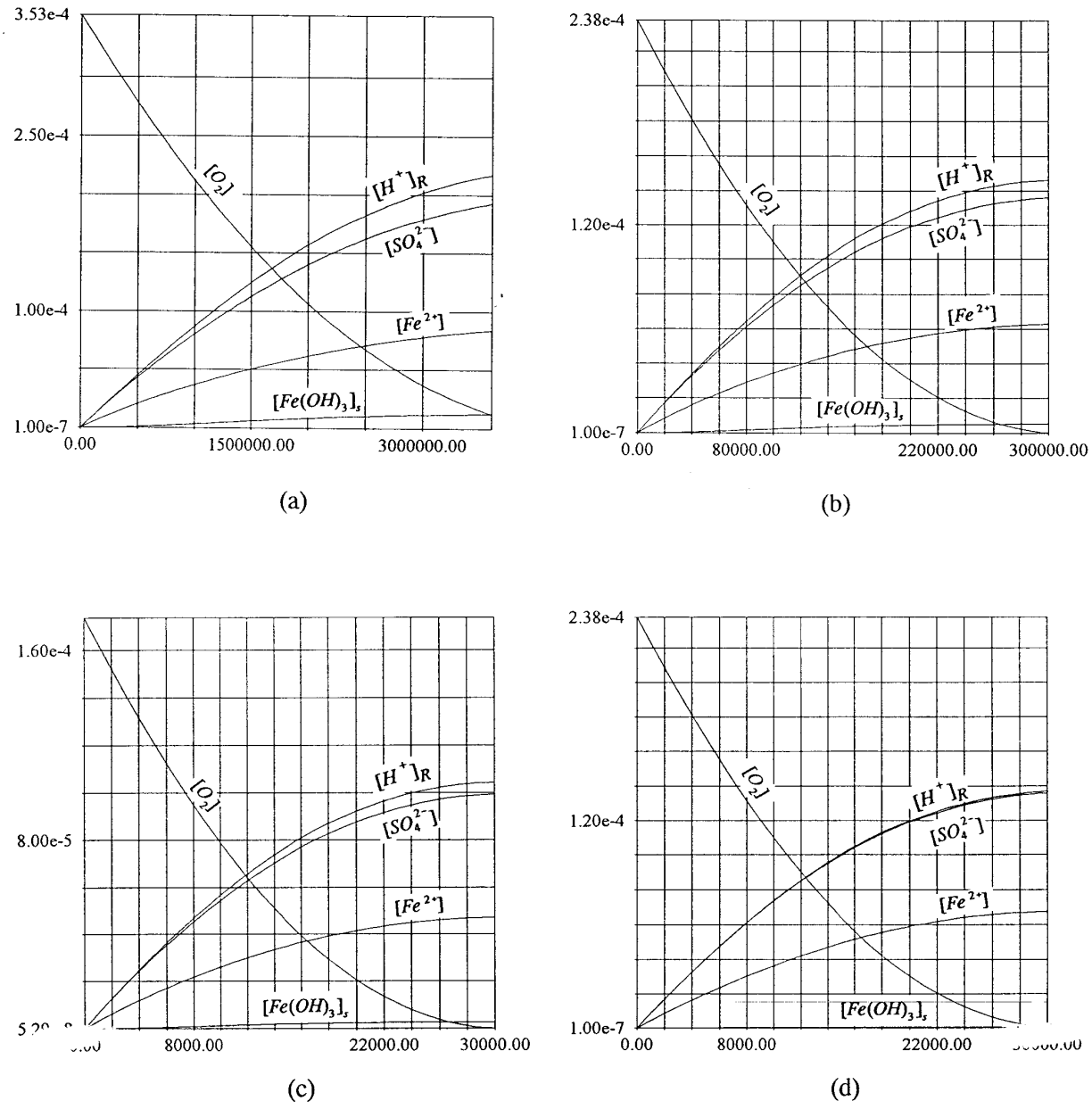


Fig. A5. The consumption of dissolved oxygen at pH=5.5 for different values of S/V and different temperatures. (a) S/V=1m$^2$/l, T=283 K; (b) S/V=1m$^2$/l, T=303 K; (c) S/V=1m$^2$/l, T=323 K; (d) S/V=10m$^2$/l, T=303 K. Horizontal axis: time in seconds; vertical axis: concentration in moles per litre (3 000000 s=35 days).

## APPENDIX B

### Numerical solutions by the finite elements method

Figs. B1 and B2 present numerical results for the two piles, 12 m and 18 m high, analyzed in Scenario 1 in Section 5.1. The numerical values are obtained for trapezoidal piles with the base 100 meters long. The maximum temperatures in both cases are by about 1$^{o}$C lower than the values obtained analytically. This difference is due to the cooling effect resulting from the heat escape through the side boundaries. The numerical results confirm the results of the scaling analysis.

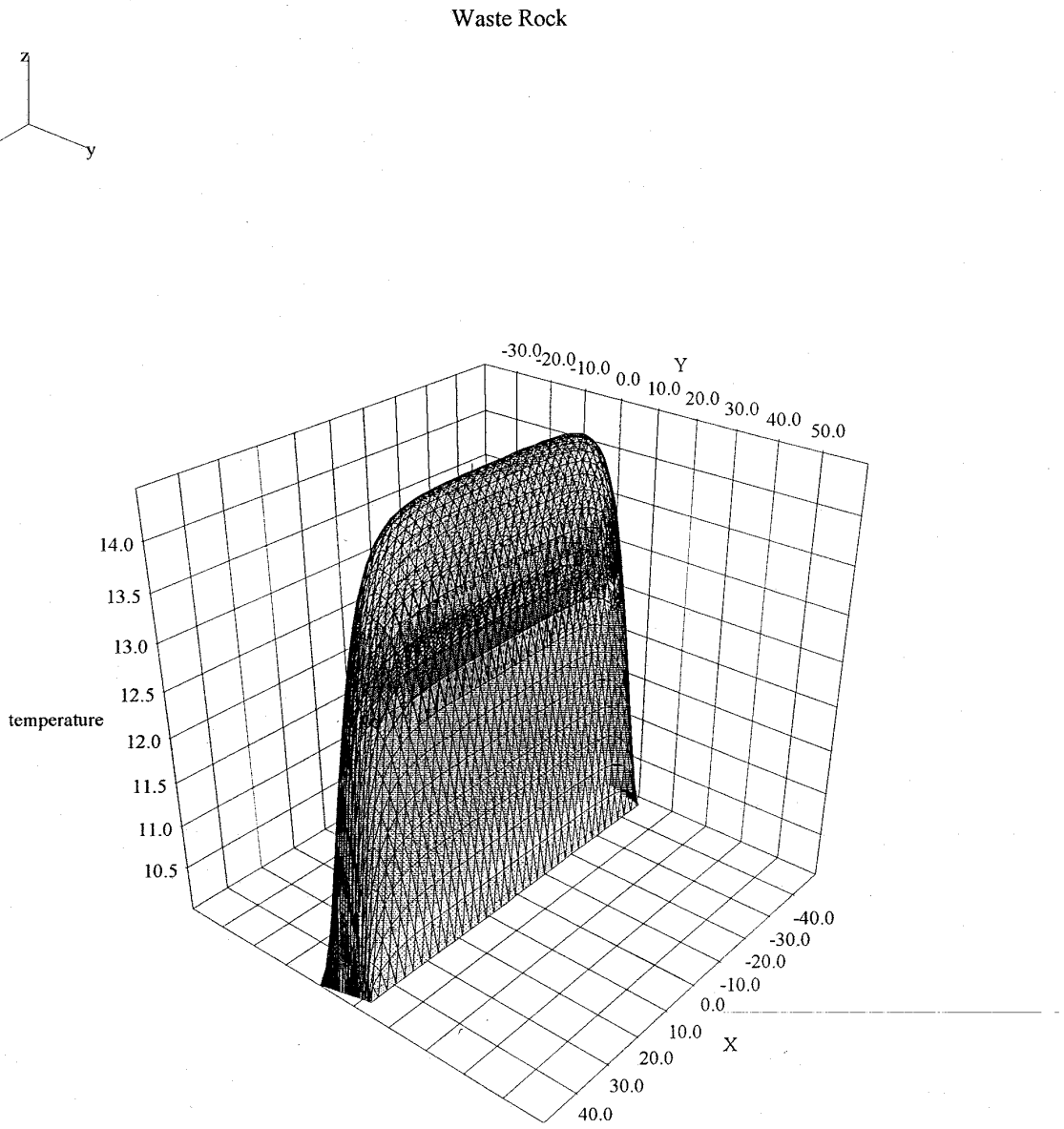


Fig. B1(a). Temperature profile for the pile 12 m high (y-axis) and 100 m long (x-axis); L=6 m; all entry data listed in Table 5.1. Analytical results are presented in Fig. 5.2.

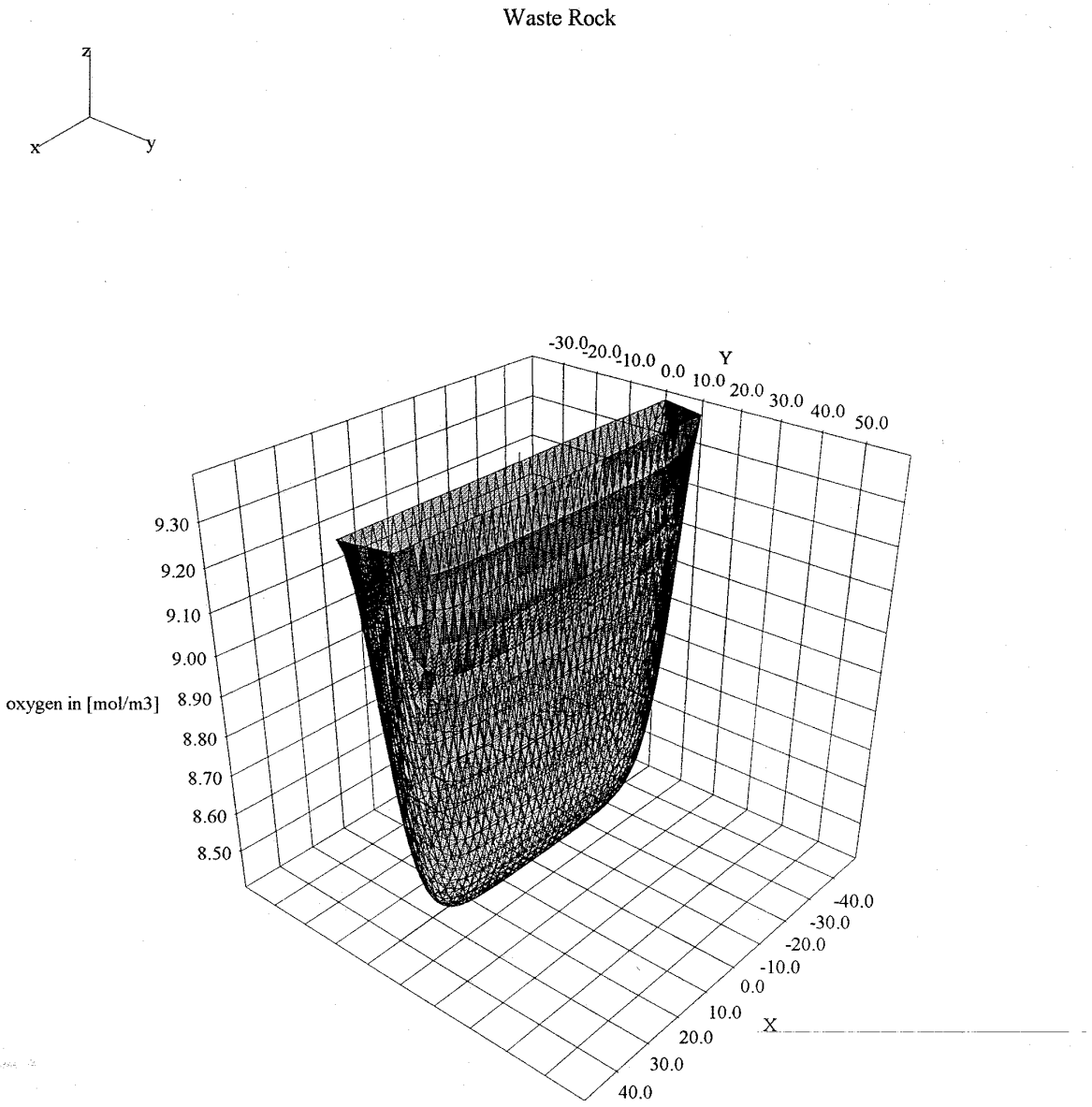


Fig. B1(b). Oxygen concentration profile for the pile 12 m high (y-axis) and 100 m long (x-axis) (L=6 m; all entry data listed in Table 5.1.

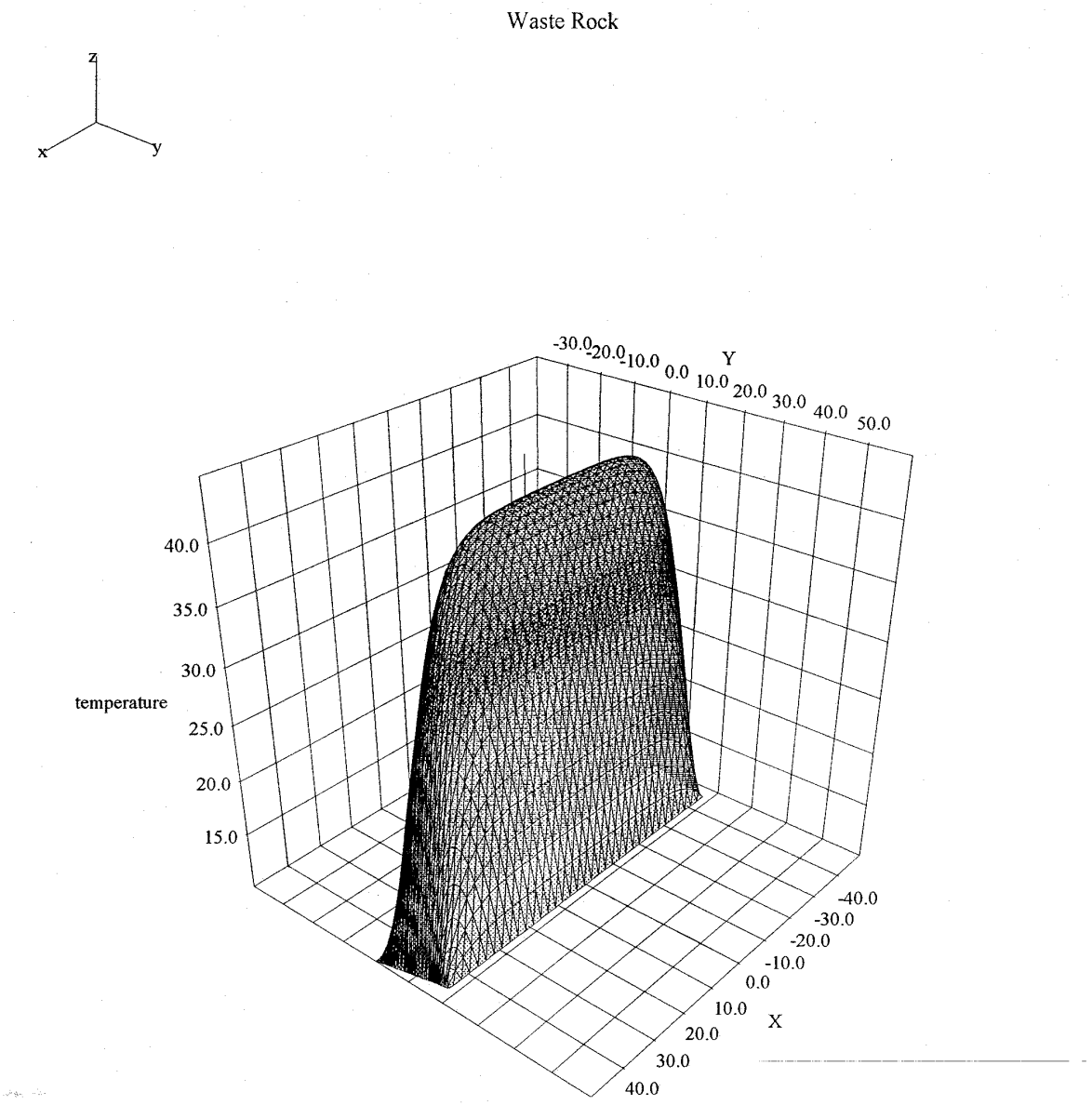


Fig. B2(a). Temperature profile for the pile 18 m high (y-axis) and 100 m long (x-axis); L=9m; all entry data listed in Table 5.1. Analytical results are presented in Fig. 5.3.

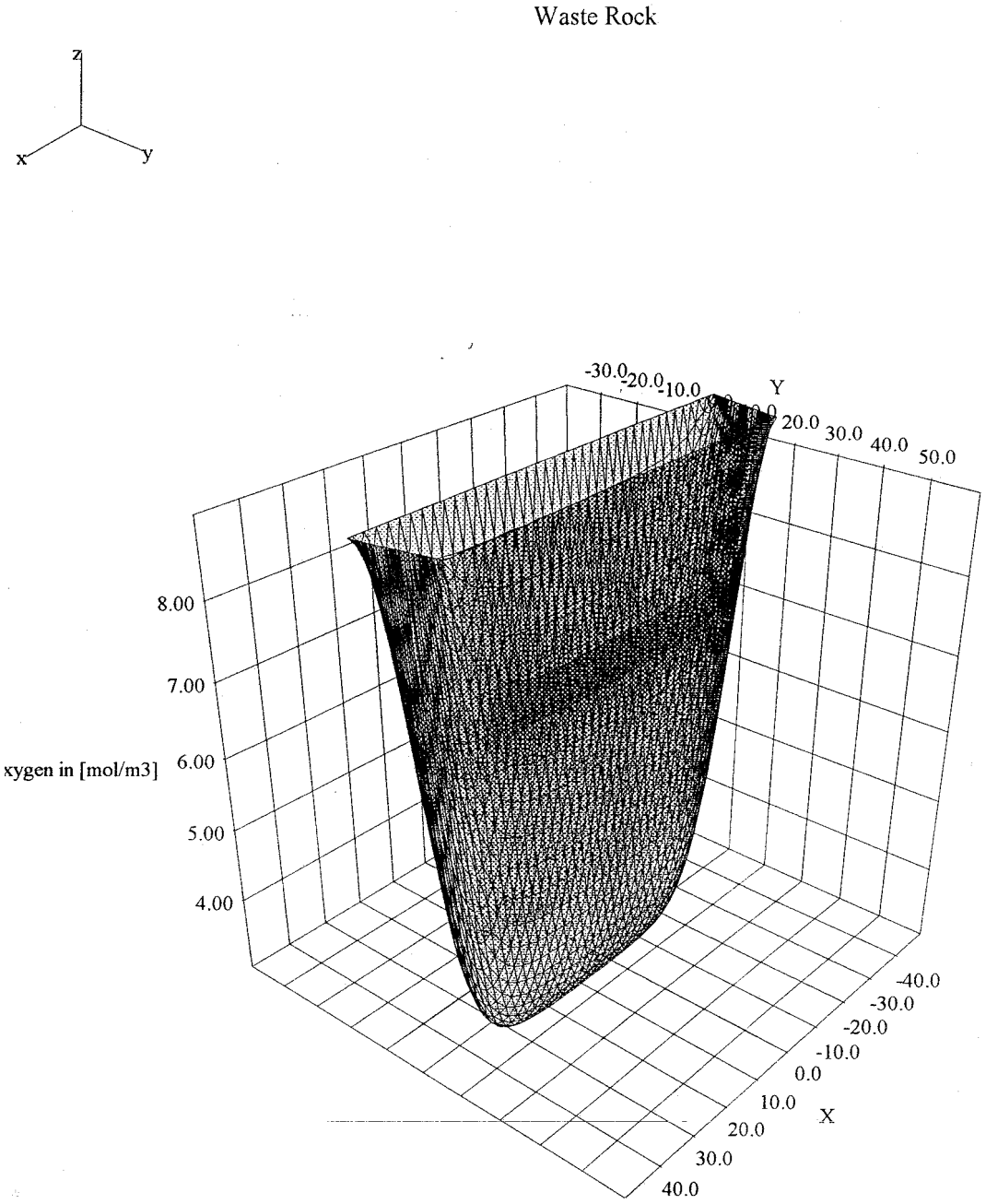


Fig. B2(b). Oxygen concentration profile for the pile 18 m high (y-axis) and 100 m long (x-axis) ; L=9m; all entry data listed in Table 5.1.

## REFERENCES

[Al] R. Albright
in Proceedings of Acid Mine Drainage Workshop; Environment Canada and Transport Canada, Halifax, NS, p. 146, 1987.

[ApK] R.J. Applegate and M.Kraatz
"*Rehabilitation of Rum Jungle Mine*"
Proc. MEND Conf, Montreal 1991.

[Ar] R. Aris
*A Mathematical Theory of Reacting and Diffusing Systems*
Wiley 1981.

[BaZ] G.I. Barenblatt and Y.B.Zeldovich
A. Rev. Fluid Mech. **4**, 285 (1972)

[BaO] J.E. Bailey and D.F.Ollis
"*Biochemical engineering fundamentals*"
McGraw-Hill, New York 1986.

[Be] T. Beer
*Applied Environmetrics Hydrological Tables*
Applied Environmetrics, Victoria, Australia, 1991.

[BeK] B.B. Benson and D.Krouse, Jr.,
*"The concentration and isotopic fractionation of gases dissolved in fresh water in equilibrium with the atmosphere, I Oxygen"*
Limnol. Oceanog., **25**, 662 (1980).

[BeP] J.W. Bennet and G.Pantelis
"*Construction of a waste rock dump to minimise acid mine drainage a case study*"
Proc. MEND Conf., Montreal 1991.

[BeR] J. W. Bennett and A.I.M.Ritchie
"*Measurements of the transport of oxygen into two rehabilitated waste rock dumps*"
Proc. MEND Conf., Montreal 1991.

[BoB] F.C. Boogerd, C. van den Beemd, T. Stoelwinder, P.Bos and J.G. Kuenen
"*Relative contributions of biological and chemical reactions to the overall rate of pyrite oxidation at temperatures between 30°C and 70°C*"
Biotechnology and Bioengineering **38**, 109 (1991).

[BrC] British Columbia Acid Mine Drainage Task Force
*"Acid Rock Drainage Technical Guide"*
BC AMD Task Force Report, 1989.

[CaG] F.T. Carruccio, G. Geidel and M.Pelletier
J. Energy (Amer. Soc. Civil Engineers), **107**, (1981).

[CaW] M.C. Campbell, D.Wadden, A.Marchbank, R.G.L.McCready and G.Ferroni
"*In-place leaching of uranium at Denison Mines Ltd.*"
Proc. IAEA Meeting, Vienna 1985.

[CdO] J. Chadam and P.Ortoleva
Earth Science Reviews, **29**, 175 (1990).

[Ch] F. Chaiken, private communication (1992).

[ChB] K. Ye Cheng and P.L. Bishop
J. Air&Waste Manage. Assoc., **42**, 164 (1992).

[Co] W.R. Cowan
Hazardous Mat. Mgmt., **3**, 12 (1991)

[CoR1] Coastech Research
*"Investigation of Prediction Techniques for Acid Mine Drainage"*
MEND Project, West Vancouver, BC, Canada, 1989.

[CoR2] Coastech Research
"Acid Rock Drainage Prediction Manual: A manual of Chemical Evaluation Procedures for the prediction of Acid Generation from Mine Wastes"
Mend Project, North Vancouver, BC, Canada 1990.

[Da] S. Day
*"Long term kinetic acid generation studies, Cinola project"*
B.C. AMD Task Force, 1993.

[DaR1] G.B. Davis and A.I.M. Ritchie
"*A model of oxidation in pyritic mine wastes: part 1: equations and approximate solutions*"
Appl. Math. Modelling, **10**, 314 (1986).

[DaR2] G.B. Davis and A.I.M. Ritchie
"*A model of oxidation in pyritic mine wastes: part: comparison of numerical and approximate solutions*"
Appl. Math. Modelling, **10**, 323 (1986).

[DaR3] G.B. Davis and A.I.M. Ritchie
"*A model of oxidation in pyritic mine wastes: part 3: importance of particle size distribution*"
Appl. Math. Modelling **11**, 417 (1987)

[DrA] D.W. Drott and R. Aris,
*"Communications on the theory of diffusion and reaction-I A complete parametric study of the first-order, irreversible exothermic reaction in a flat slab of catalyst".*
Chem. Engng. Sci. **24**, 541, (1969).

[DuB] D.W. Duncan and A. Bruynsteyn
"*Determination of the Acid Production Potential of Waste Materials*"
Metallurgical Society of AIME Annual Meeting, New Orleans (1979).

[DuD] J.G. Dunn, G.C. De and P.G. Fernandez
"*The effect of experimental variables on the multiple peaking phenomenon observed during the oxidation of pyrite*"
Thermochimica Acta, **135**, 267 (1988).

[ErH] P.M. Erickson, R.W. Hammack and R.L.P. Kleinman
*"Prediction of acid drainage potential in advance of mining"*
in Control of Acid Mine Drainage, USBM IC 9027.

[Es] H. Ese
*"Acidic mine drainage from the Killingdal Mine Norway"*
Proc. MEND Conf., Montreal 1991.

[Fe] K.D. Ferguson
*"Static and Kinetic Methods to Predict Acid Mine Drainage"*
Env. Canada, 1985.

[FeE] K.D. Ferguson and P.M. Erickson
*"Approaching the AMD Problem-from Prediction and early Detection"*
In. Proc. Int. Conf. on Control of Environmental Problems from Metal Mines, 1988, Roros, Norway.

[FeE1] K.D. Ferguson and P.M. Erickson
*"Will It Generate Acid? An Overview of Methods to Predict Acid Mine Drainage"*

[FeMe] K.D. Ferguson and P.E. Mehling
*"Acid Mine Drainage in B.C. The Problem and Search for Solutions"*
Environment Canada, 1986.

[FeM] K.D. Ferguson and K.A. Morin
*"The prediction of Acid Rock Drainage - Lesson from the Database"*
Environment Canada Report, 1992.

[Ga] D.M. Galbraith
*"The mount Washington acid mine drainage reclamation project"*
Proc. MEND Conf., Montreal 1991.

[Ge] P. Gelinas and R.Guay
*"Acid Mine Drainage Generation from a Waste Rock Dump and Evaluation of Dry Covers Using Natural Minerals: La Mine Doyon Case Study"*
MEND Report (1990)

[Ge] P. Gelinas, private communication (1993)

[Go] B. Godin, private communication

[Gol] M.B. Goldhaber
*"Experimental study of metastable sulpfur oxyanion formation during pyrite oxidation"*
Am. J. Sci. 283, 193 (1983).

[Ha] Sophie Bierens de Haan
*"A review of the rate of pyrite oxidation in aqueous systems at low temperature"*
Earth-Science Reviews **31**, 1, (1991).

[HoS] George R. Holdren, Jr. and Patricia M. Speyer
*"Reaction rate - surface area relationships during the early stages of weathering - I. Initial observations"*
Geochimica et Cosmochimica Acta **49**, 675 (1985).

[HwS] C.C. Hwang, R. C. Streeter, R.K. Young and Y.T. Shah
*"Kinetics of the ozonation of pyrite in aqueous suspension"*
Fuel **66**, 1574 (1987).

[KeW1] G.H. Kelsall and R.A. Williams
*"Electrochemical behavior of ferrosilicides ($Fe_xSi$) in Neutral Alkaline Aqueous Electrolytes. I. Thermodynamics of Fe-Si-$H_2O$ systems at 298 K"*
J. Electrochem. Soc. **138**, 941 (1991).

[KoB] A. Kok, N. Bolt and J.H.N. Jergersma
KEMA Sci.&Tech. Reports **7**, 63 (1989)

[Kw] Y.T.J. Kwong
*"Acid generation in waste rock as exemplified by the Mount Washington mine site, B.C., Canada"*
Proc. MEND Conf., Montreal 1991.

[Las] Antonio C. Lasaga
*"Chemical Kinetics of Water-Rock Interactions"*
Journal of Geophysical Research **89**, 4009, (1984).

[LawR] R.W. Lawrence, G.M. Ritcey, G.W. Poling, P.B. Marchant
"*Strategies for the Prediction of Acid Mine Drainage"*
Proceedings of the 13th Mine Reclamation Symposium, Ministry of Energy, Mines and Petroleum Resources; Victoria, 1989.

[LeW] J.H. Levy and T. J. White
*"The reaction of pyrite with water vapour"*
Fuel **67**, 1336 (1988)

[LGI] R. Lefebvre, P. Gelinas and D. Isabel
*"Heat transfer during acid mine drainage production in a waste rock dump, La Mine Doyon (Quebec)"*
MEND Report 1.14.2

[Low] Richard T. Lowson
*"Aqueous Oxidation of Pyrite by Molecular oxygen"*
Chemical Reviews **82**, 461 (1982).

[Lu] George W. Luther III
*"Pyrite oxidation and reduction: Molecular orbital theory considerations"*
Geochimica et Cosmochimica Acta **51**, 3193 (1987).

[LuF] G.W. Luther III, T.G. Ferdelman, J.E. Kostka, E.J. Tsamakis and T.M. Church
*"Temporal and spatial variability of reduced sulpfur species and porewater parameters in salt marsh sediments"*
Biogeochemistry **14**, 57 (1991).

[MaR1] C.T. Mathews and R.G. Robins
Australais. Ins. Mining Metall. **242**, 47 (1972).

[MaR2] C.T. Mathews and R.G. Robins
Aust. Chem. Eng. **15**, 19 (1975).

[MaR3] C.T. Mathews and R.G. Robins
Aust. Chem. Eng. **13**, 129 (1972).

[McC] R. McCandless
private communication, 1993.

[McK] Michael A.McKibben and Hubert L. Barnes
*"Oxidation of pyrite in low temperature acidic solutions: Rate laws and surface textures"*
Geochimica etCosmochimicaActa **50**, 1509-20 (1986).

[MiS] F.J. Millero, S.Sotolongo and M.Izaguirre
"The oxidation kinetics of Fe(II) inSeawater"
Geochimica etCosmochimicaActa **51**, 793-801 (1987).

[MoJ] K. A. Morin, E. Gerencher, C.E. Jones, D. Konasewich and J.R. Harries
*"Critical literature review of acid drainage from waste-rock"*
Nothwest Geochem, 1990.

[MoM] John W. Morse, Frank J.Millero, Jeffrey C.Cornwell and D.Rickard
*"The chemistry of the HydrogenSulfide and IronSulfide Systems inatural Waters"*
Earth-Science Review**24**, 1 (1987).

[MsH] Carl O. Moses, Alan T.Herlihy, Janet. S. Herman and Aaron L. Molls
*"Ion-chromatographic analysis of mixtures of ferrous and ferric iron"*
Talanta **35**, 15 (1988).

[MsH] Carl O. Moses and Janet S. Herman
*"Homogeneous Oxidation Kinetics of Aqueous Ferrous Iron atircumneutral pH"*
Journal of Solution Chemistry**18**, 705 (1989).

[MsH] Carl O. Moses and Janet S. Herman
*"Pyrite oxidation atcircumneutral pH"*
Geochimica etCosmochimicaActa **55**, 471 (1991).

[MsN] Carl O. Moses, D.Kirk Nordstrom, Janet S. Herman and Aaron L. Mills
*"Aqueous pyrite oxidation by dissolved oxygen and by ferric iron"*
Geochimica etCosmochimicaActa **51**, 1561 (1987).

[Ni] R.V. Nicholson, private communication (1993).

[NiG] Ronald V. Nicholson, Robert W.Gillham and Eric J.Reardon
*"Pyrite oxidation in carbonate-buffered solution:. 1. Experimentainetics"*
Geochimica etCosmochimicaActa **52**, 1077 (1988)

[NiG] Ronald V. Nicholson, Robert W. Gillham and Eric J. Reardon
*"Pyrite oxidation in carbonate-buffered solution:. 2. Rate control by oxide coatings"*
Geochimica et Cosmochimica Acta" **54**, 395 (1990)

[NiP] G. Nicolis and I. Prigogine
*Self-Organization in Nonequilibrium Systems*
Wiley, 1977.

[NiS] R.V. Nicholson and J.M. Scharer
*"Laboratory Studies of Pyrrhotite Oxidation Kinetics"*
preprint

[No] D.K. Nordstrom
"Aqueous pyrite oxidation and the consequent formation of secondary iron minerals" in Acid sulfate weathering: pedogeochemistry and relationship to manipulation of soil materials, Soil Science Soc. Amer. Press, Madison, 1982.

[NoD] Nolan, Davis and Associates
*Heath Steele Waste Rock Study*
MEND Report 2.23.1a, 1992

[NoJ] Nordstrom D.K., E.A. Jenne and J.W. Ball
*"Redox equilibria of iron in acid mine waters"*,
ACS Symposium Series **93**, 51-59 (1979).

[Ot1] M. Otwinowski
*"A thermodynamic model for the spontaneous heating and combustion of coal. I: Elementary exothermic processes"*
Fuel, submitted; also Alberta Energy Report, Edmonton 1991.

[Ot2] M. Otwinowski
*"A thermodynamic model for the spontaneous heating and combustion of coal. II: Reaction-diffusion model"*
Fuel, submitted; also Alberta Energy Report, Edmonton 1991.

[Ot3] M. Otwinowski
*Static and Dynamic Patterns in Equilibrium and Nonequilibrium Systems*
in Nonlinear Structures in Physical Systems, Chaos Pattern formation and Waves ,Springer, 1990

[OtL1] M. Otwinowski, W.G. Laidlaw and R. Paul
*"Structural instability of the Brusselator model with reversible chemical reactions"*
Can. J. Phys. **68**, 743 (1990)

[OtL2] M. Otwinowski, W.G.Laidlaw and R. Paul
*"Explicit solutions to a class of nonlinear diffusion equations"*
Phys. Lett. **124**, 149 (1988).

[PaR] G. Pantelis and A.I.M. Ritchie
*"Macroscopic transport mechanisms as a rate-limiting factor in dump leaching of pyrite ores"*
Appl. Math. Modelling **15**, 136 (1991)

[PrL] I. Prigogine and R.Lefevre
J. Chem. Phys. **48**, 1695 (1968).

[PrT] William A.Pryor and Umberto Tonnellato
*"Nucleophilic Displacements at Sulfur. III. The Exchange of Oxygen-18 between Sodium Thiosulfate-$^{18}O$ and Water"*
Journal of the American Chemical Society **89**, 3379 (1967).

[Res] Rescan Env. Services Ltd.
*"Kutcho Creek project. Acid generation testwork"*
Report, 1990, Vancouver, Canada.

[ScG] J.M. Scharer, V. Garga, R. Smith and B.E. Halbert
*"Use of Steady-State Models for Assessing Acid Generation in Pyritic Mine Tailings"*
in Proceedings of the 2nd International Conference on Abatement, Montreal, p. 211, Tome 2, 1991.

[Sch} A. Schmal
Ph.D. Theses, Utrecht, 1983.

[ScD] A. Schmal, J.H.Duyzer and J.W. van Heuven
Fuel **64**, 1969 (1985)

[Se] Senes Consultants
*"Description of RATAP.BMT3 Component Modules"*
Report, 1991.

[SiS] P.C. Singer and W.Stumm
*"Acidic Mine Drainage: The Rate Determining Step"*
Science **167**, 1121 (1970).

[SnL] G.A. Singleton and L.M. Lavkulich
Soil Science **42**, 984 (1978).

[SoS] A.A. Sobek, W.A. Schuller, J.R. Freeman and R.M. Smith
US EPA Report; EPA 600/2-78-054, 1978

[St] W. Stumm ed.,
*"Aquatic Chemical Kinetics. Reaction Rates of Processes in Natural Waters"*
Wiley, 1991.

[StL1] W. Stumm and G.F. Lee
Schwei. Z. Hydrol. **22**, 295 (1960).

[StL2] W. Stumm and G.F. Lee
Ind. Eng. Chem. **53**, 143 (1961).

[StM] W. Stumm and J.J. Morgan,
*"Aquatic Chemistry. An introduction Emphasizing Equilibria in Natural Waters"*
Wiley, 1986.

[Sul] P.J. Sullivan and A.A. Sobek
Minerals and the Environment **4**, 9 (1982)

[SyT] Synergetic Technology
*"Quantitative Analysis of Chemical and Biological Kinetics for the Acid Mine Drainage Problem"*
MEND Report (1993)

[TaW2] B.E. Taylor and M.C. Wheeler and D.K. Nordstrom
*"Stable isotope geochemistry of acid mine drainage: Experimental oxidation of pyrite"*
Geochimica et Cosmochimica Acta **48**, 2669 (1984)

[WaK] E. I. Wallick, H.R. Krouse and A. Shakur
*"Environmental isotopes: principles and applications in ground water geochemical studies in Alberta, Canada"*
in First Can. Conf. on Hydrology, 1984.

[We] Bernhard Wehrli
*"Redox reactions of metal ions at mineral surfaces"*
in Aquatic Chemical Kinetics W. Stumm ed., Willey, 1990.

[WhJ] W.W. White III and T.H. Jeffers
*"Chemical predictive modelling of acid mine drainage from metallic sulfide-bearing waste rock"*
U.S. Department of Interior, Bureau of Mines, 1992.

[WiR] C.L. Wiersma and J.DRimstidt
*"Rates of reaction of pyrite andmarcasite with ferric iron at pH 2"*
Geochimica etCosmochimicaActa **48**, 85 (1984)

[YaW] E.K. Yanful,K.G. Wheeland, C.Luc and N.Kuyucak
*"Overview ofNoranda Research on Prevention and Control of Acid Mine Drainage"*
Environmental Workshop 1991, Australian Mining Industry Council

[ZiM] Z.D. Zivkovic, N.Molosavljevic and JSestak
*"Kinetics and Mechanism of Pyrite Oxidation"*
ThermochimicaActa **157**, 215 (1990).